No single model for supersized eruptions and their magma bodies

Colin J. N. Wilson[1]✉, *George F. Cooper*[2], *Katy J. Chamberlain*[3], *Simon J. Barker*[1], *Madison L. Myers*[4], *Finnigan Illsley-Kemp*[1] *and Jamie Farrell*[5]

Abstract | Supereruptions are the largest explosive volcanic eruptions on Earth. They generate catastrophic, widespread ash-fall blankets and voluminous ignimbrites, with accompanying caldera collapse. However, the mechanisms of generation, storage and evacuation of the parental silicic magma bodies remain controversial. In this Review, we synthesize field, laboratory and petrological evidence from 13 Quaternary supereruptions to illustrate the range of diversity in these phenomena. Supereruptions can start mildly over weeks to months before escalating into climactic activity, or go into vigorous activity immediately. Individual supereruptions can occupy periods of days to weeks, or be prolonged over decades. The magmatic sources vary from single bodies of magma to multiple magma bodies that are simultaneously or sequentially tapped. In all 13 cases, the crystal-rich (>50–60% crystals), deep roots (>10 km) of the magmatic systems had lifetimes of tens of thousands to hundreds of thousands of years or more. In contrast, the erupted magmas were assembled at shallower depths (4–10 km) on shorter timescales, sometimes within centuries. Geological knowledge of past events, combined with modern geophysical techniques, demonstrate how large silicic caldera volcanoes (that have had past supereruptions) operate today. Future research is particularly needed to better constrain the processes behind modern volcanic unrest and the signals that might herald an impending volcanic eruption, regardless of size.

Supereruptions
Events that discharge more than 1×10^{15} kg of magma (450 km^3 or > ~ 1,000 km^3 of pumice and ash) in a single eruption.

[1]*School of Geography, Environment and Earth Sciences, Victoria University of Wellington, Wellington, New Zealand.*

[2]*School of Earth and Environmental Sciences, Cardiff University, Cardiff, UK.*

[3]*Environmental Sustainability Research Centre, University of Derby, Derby, UK.*

[4]*Department of Earth Sciences, Montana State University, Bozeman, MT, USA.*

[5]*Department of Geology and Geophysics, University of Utah, Salt Lake City, UT, USA.*

✉*e-mail: colin.wilson@vuw.ac.nz*

https://doi.org/10.1038/s43017-021-00191-7

Supereruptions[1] are the largest explosive volcanic eruptions and represent the most catastrophic endmember of terrestrial natural hazards[2–4]. Although rare globally (roughly one per 100,000 years[1–3]), supereruptions reach volumes that exceed 1–2 orders of magnitude greater than any historic explosive eruption and are, inevitably, associated with large-scale caldera collapse. These cataclysmic events offer unique insights into the diversity of large-scale magmatic processes that occur in the Earth's crust[5–7]. The causes and triggers of such extremely large eruptions and the behaviour of their parental magmatic systems are often explained in the literature through generalized models[8–17]. However, consideration of available evidence suggests that there is great diversity in almost all aspects of these phenomena, from the timescales of magma accumulation and eruption, to the architecture of the underlying magmatic systems.

The arbitrary (yet, widely used) term supervolcano[4] is often used to define a large silicic caldera volcano that has generated a supereruption, and is also sometimes referred to as a supereruptive centre. However, these terms can be misleading, as large explosive eruptions are never isolated events in the history of a volcanic and/or magmatic system. There are usually records of numerous smaller events prior to and following the supersized event[18–22], except in some cases, such as Toba[23], Indonesia, for example. Such smaller events yield snapshots of the evolving magma system and help to constrain what process led to the supereruption. However, models for the growth and rupture of magma chambers, especially to super sizes[13–17], are currently hampered by an inability to explain why a magmatic system should release small amounts of magma during its growth towards giant size. To date, there are no unique explanations for the mechanisms, timings and extreme volumes of supereruptions.

All large silicic systems (not just those with calderas or eruptions of super size) have complex roots that are ultimately fed by mantle-derived basaltic magmas[6–8,11]. Minor amounts of these deeper, less evolved basaltic magmas can reach the surface in some eruptions, for example, in the form of mafic enclaves or late-stage pyroclastic deposits[24–28]. Unusually high fluxes of basaltic magma are the fundamental control in fuelling the supersized magmatic systems[7,29,30], through their basic role in generating silicic melts through crystal fractionation and/or by melting of crustal rocks. However, the controls on whether small to large volumes of silicic

Key points

- Field studies demonstrate that supereruptions show great diversity in their style, rapidity of onset, duration of eruption, triggering mechanisms for eruption onset and caldera collapse.
- The magma reservoirs from which supereruptions are sourced are comparably diverse, with examples of both single and multiple bodies, each of which can be compositionally zoned or convectively mixed.
- Past supereruptions serve to define a supervolcano, but this arbitrary term does not constrain the modern or future behaviour of that particular volcano.
- Geophysical imaging of magma storage regions at modern, large silicic volcanoes (including supervolcanoes) is broadly consistent with petrological inferences, but imaging resolution is insufficient to identify small, melt-dominant bodies capable of supplying eruptions.
- Large silicic volcanoes often undergo periods of unrest, consisting of elevated seismicity, ground deformation and gas emissions. Monitoring of these systems must contend with the challenge of differentiating 'normal' unrest from pre-eruptive signals.
- Further work is needed to better understand the processes that cause these long-lived magmatic systems to accumulate eruptible magma bodies and the subsequent tipping points that cause these to erupt.

magma erupt or stay at depth to build plutons are still debated[5,31]. In addition, there is a growing consensus that, for most of their histories, large silicic magmatic systems reside dominantly in a largely crystalline state termed mush. In this widely adopted mush model[10,24,32,33], separation of melt-dominant material into shallow bodies is considered a necessary precursor to rhyolitic eruptions (of whatever size). If the mush itself is mobilized wholesale by thermal inputs, it can also contribute in large volumes to crystal-rich dacitic or rhyolitic material (for example, Cerro Galán, Argentina, and Ongatiti, New Zealand).

Although minor amounts of effusive activity generally occur before or after a supereruptive event to generate lava flows[34], the supereruption record is entirely represented by pyroclastic deposits. Even the largest lava flows associated with large silicic magmatic systems (for example, at Yellowstone[18]) only reach volumes of tens of cubic kilometres. In comparison, pyroclastic products of the largest eruptions achieve up to the 1,000–10,000 cubic kilometres range[1]. The magmas that are discharged in supereruptions are broadly silicic and cover a range in compositions from (generally) crystal-richer dacites (65–71 wt% SiO_2) to (generally) crystal-poorer rhyolites (71–78 wt% SiO_2). Although typically erupted from storage bodies at shallow depths (<5–10 km), it has long been recognized that these magma compositions reflect magmatic systems that span a wide range of depths in the local crust (~5–60 km)[6–8,11]. Two closely linked kinds of pyroclastic deposits are important in the Quaternary supereruption record: widespread but thin fall deposits that can occur on a continental or global scale (FIG. 1) and ignimbrite laid down from pyroclastic flows that are tens to hundreds of metres thick and extend out ~100–150 km from source[34]. In addition, evacuation of the vast magma reservoir leads inevitably to caldera collapse, and the substantial volumes of eruptive material are inferred to accumulate in the resulting caldera depression as infill[1].

Since 2000, there has been an abundance of new field and analytical studies undertaken on individual supereruption deposits that make it apparent that there is great diversity in these phenomena, in contrast to simplifications required in numerical models. These geological case studies, when coupled with new geophysical approaches and data, provide insights into the behaviour of Quaternary supervolcanoes and their patterns of unrest and possible eruption that are of great interest and relevance to modern society.

In this Review, we highlight the diversity in behaviour of the currently established Quaternary (last 2.6 Myr) magmatic systems that have led to supereruptions. We outline the spectrum of processes and timescales involved in the largest scales of silicic magma generation and eruption. First, we emphasize the value of field-focused studies combined with petrological data in illuminating the nature of past supereruptions and their magmatic sources. Second, we highlight the importance of linking geological studies of past events with present-day geophysical investigations as a guide to the behaviour of modern actual (or potential) supervolcanoes. Supereruptions, as defined[1–4], are simply the largest endmembers of a continuous spectrum of volcano behaviour that is recognized as the product of multiple processes acting in a complex fashion. As a result, multidisciplinary techniques are required to understand the processes in and hazards posed by future unrest or eruption.

The eruptive record

The record preserved in eruption products is invariably the most important source of information about past supereruptions and their timing. In particular, studies of the resulting deposits and juvenile material collected in the field, such as pumice, ash and crystals (FIG. 2a–c), are central to understanding the development and evacuation of parental large silicic magmatic systems. We consider all 13 established Quaternary supereruptions (TABLE 1) and focus on selected examples that are documented in detail to illustrate key points about the eruptions and their parental magma bodies. All supereruptions considered in this Review (FIG. 1) have occurred at volcanoes that are positioned on continental crust. Most are associated with subduction systems or major tectonic boundaries, apart from Yellowstone, which is associated with an intraplate hotspot (TABLE 1).

Nature of the eruption products. The nature and preservation of eruption products strongly influences the sampling of deposits and, thus, the information that can be gained about the magmatic source. Pieces of lava or individual pumices in pyroclastic deposits represent parcels of juvenile magma, so that compositional diversity or uniformity in the crystals and groundmass reflect those within the parent magma body. In contrast, compositional variations within bulk samples of pyroclastic rocks can reflect mechanical enrichment or depletion in crystals[35], or incorporation of lithic material[36] during eruption (FIG. 2a,b), and, therefore, might not reflect the magmatic source. If the groundmass material is glassy, it can be considered to represent quenched melt. Often, however, the groundmass will have crystallized (devitrified) during slow cooling and no longer reflect the original melt composition.

Caldera
A topographic depression formed through the collapse of the Earth's surface, owing to the withdrawal of large volumes of magma from the upper crust.

Supervolcano
A volcanic centre that has produced one (or more) supereruptions in the past, also referred to as a supereruptive centre.

Mush
A framework of crystals (>50–60 volume %) with interstitial melt, which forms a strong skeleton that can no longer easily flow or erupt, owing to its high viscosity.

Melt-dominant
Material separated out from the crystal mush, consisting of <40–50% crystals, that can flow and is eruptible, but which has a short lifetime within the upper crust.

Magmatic systems
Entire regions within the crust and upper mantle that feed the volcanic system, including the melt-dominant body or bodies and mushy, non-eruptible material.

Fall deposits
Deposited from high (tens of kilometres) buoyant atmospheric plumes of ash, dispersed by winds over thousands to millions of square kilometres; individual deposits are millimetres to metres in thickness.

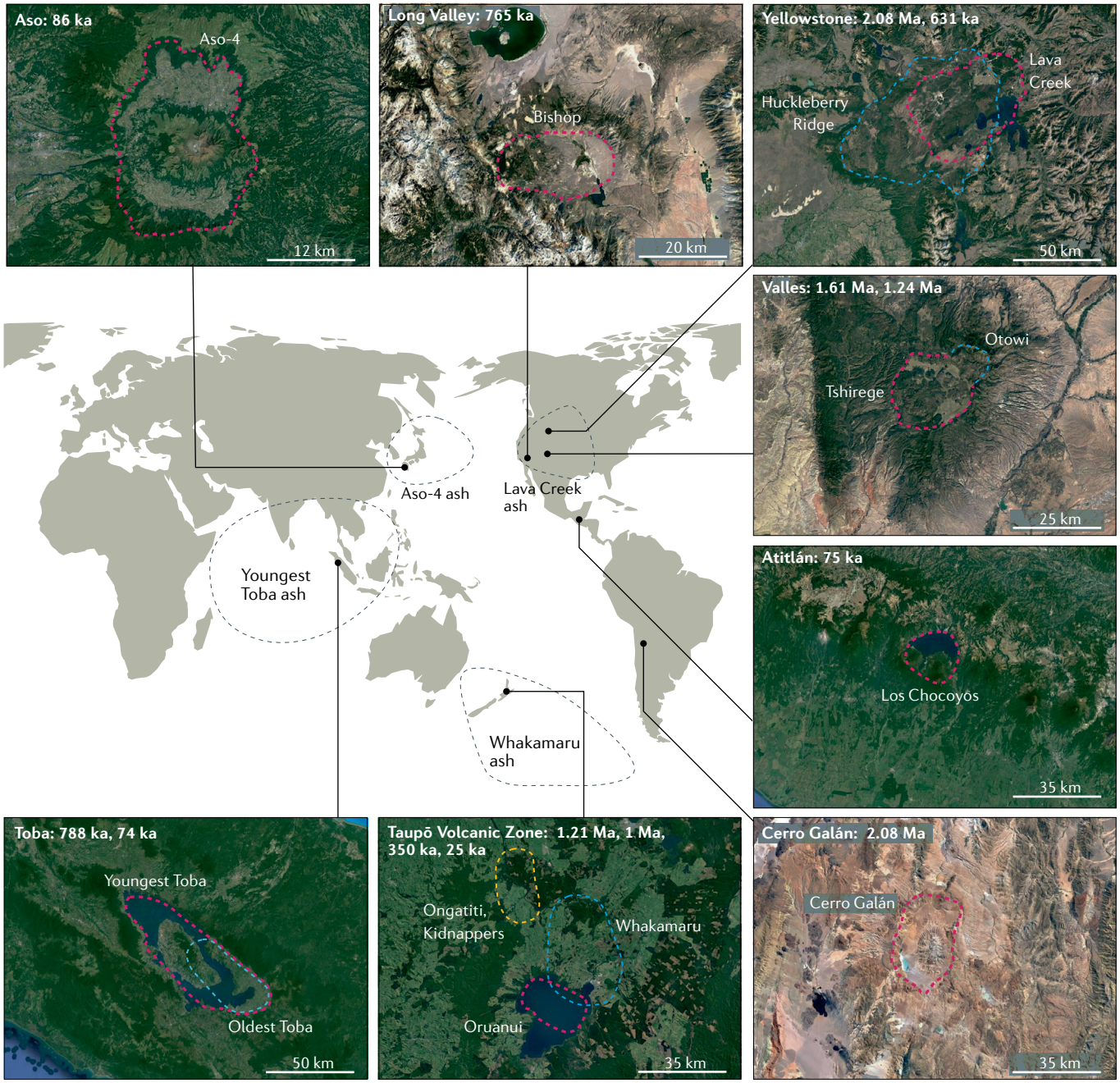

Fig. 1 | **Location maps of Quaternary supereruption locations and associated caldera outlines.** The supereruptions reviewed here come from sources roughly circling the Pacific Ocean, in association with active tectonic plate margins or hotspots. Satellite images of the source calderas are from Google Earth, with caldera outlines marked by dashed magenta, blue and yellow lines. Caldera outlines and eruptive ages are shown for Aso-4 (REFS[28,191]) from Aso (Japan); Bishop[24,36] from Long Valley (USA)[22]; Huckleberry Ridge[18] and Lava Creek[18] from Yellowstone (USA); Otowi[68] and Tshirege[99] members of the Bandelier Tuff from Valles (USA)[58]; Los Chocoyos[39] from Atitlán (Guatemala); Cerro Galán[56] from Cerro Galán (Argentina); Ongatiti[55] and Kidnappers[97] from Mangakino (New Zealand); Whakamaru[54] from Whakamaru (New Zealand); Oruanui[57] from Taupō (New Zealand); and Oldest Toba[23] and Youngest Toba[23] tuffs from Toba (Indonesia). The mapped extents of selected fall deposits are shown by black dashed regions on the world map for Aso-4 (REF.[191]), Lava Creek[37], Whakamaru[42] and Youngest Toba[38] eruptions. Images for Aso, Long Valley, Yellowstone, Valles, Cerro Galán and Taupō Volcanic Zone: map data ©2021 Google, Landsat/Copernicus. Images for Toba and Atitlán: map data ©2021 Google, SIO, NOAA, U.S. Navy, NGA, GEBCO Image: Landsat/Copernicus.

Ignimbrite
Deposits from concentrated, ground-hugging pyroclastic flows, typically metres to hundreds of metres thick, covering up to thousands to tens of thousands of square kilometres.

Ignimbrites commonly contain large enough fragments of juvenile material (pumice: FIG. 2a) so that the full nature of the magma parcel can be determined, but many ignimbrites were emplaced hot enough to compact back to solid rock under loading (weld) and devitrify, such that the pumices are flattened to lenses (fiamme: FIG. 2c) that are challenging to sample intact. In contrast, fall deposits (especially the large distal blankets

a Unwelded ignimbrite

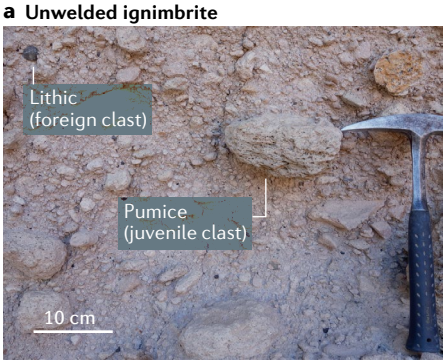

b Incipiently welded ignimbrite

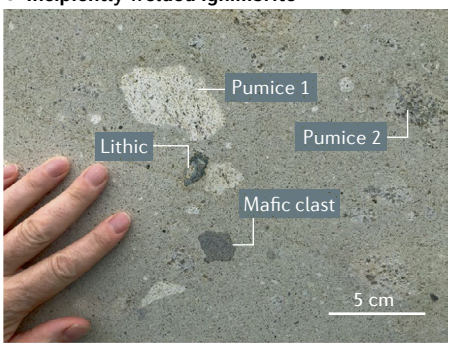

c Densely welded ignimbrite

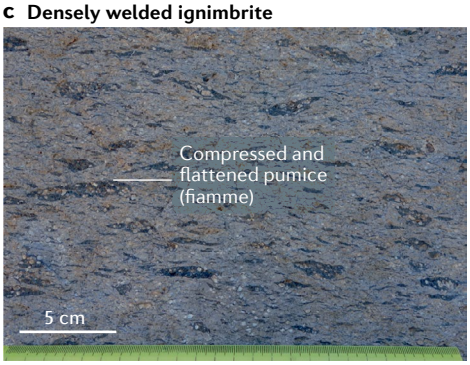

d Bishop Tuff at Chalfant quarry, California

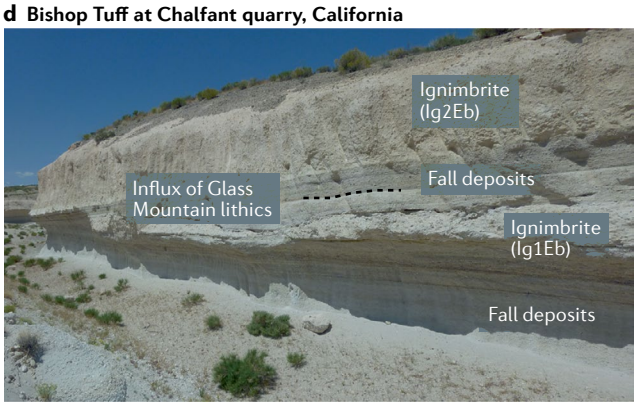

e Bishop Tuff in Owens Gorge, California

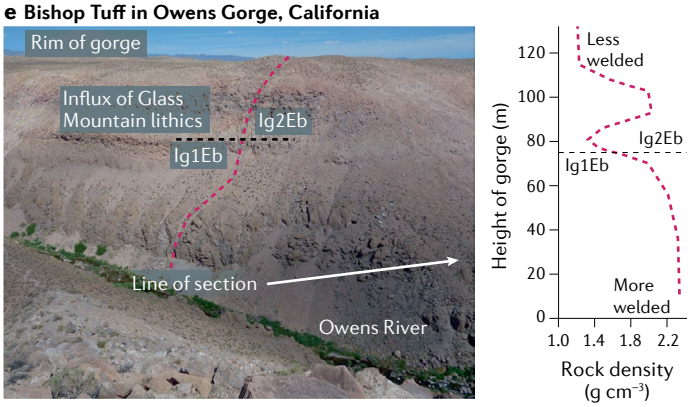

f Early Oruanui fall deposits at Taihape, New Zealand

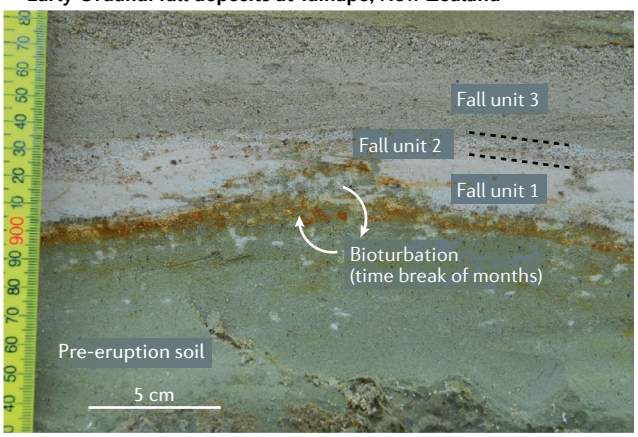

g Early Huckleberry Ridge fall deposits at Mount Everts, Wyoming

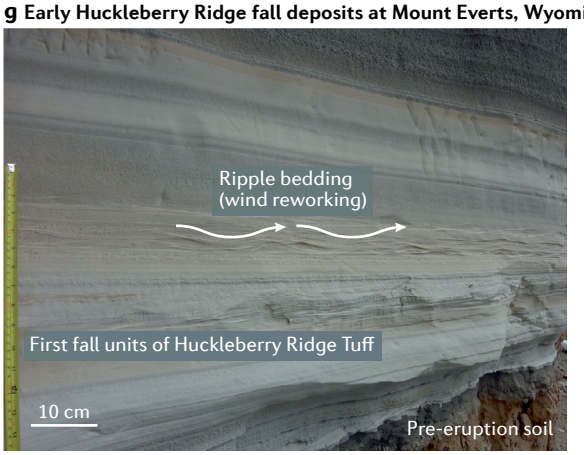

h Huckleberry Ridge ignimbrite members on the Teton River, Idaho

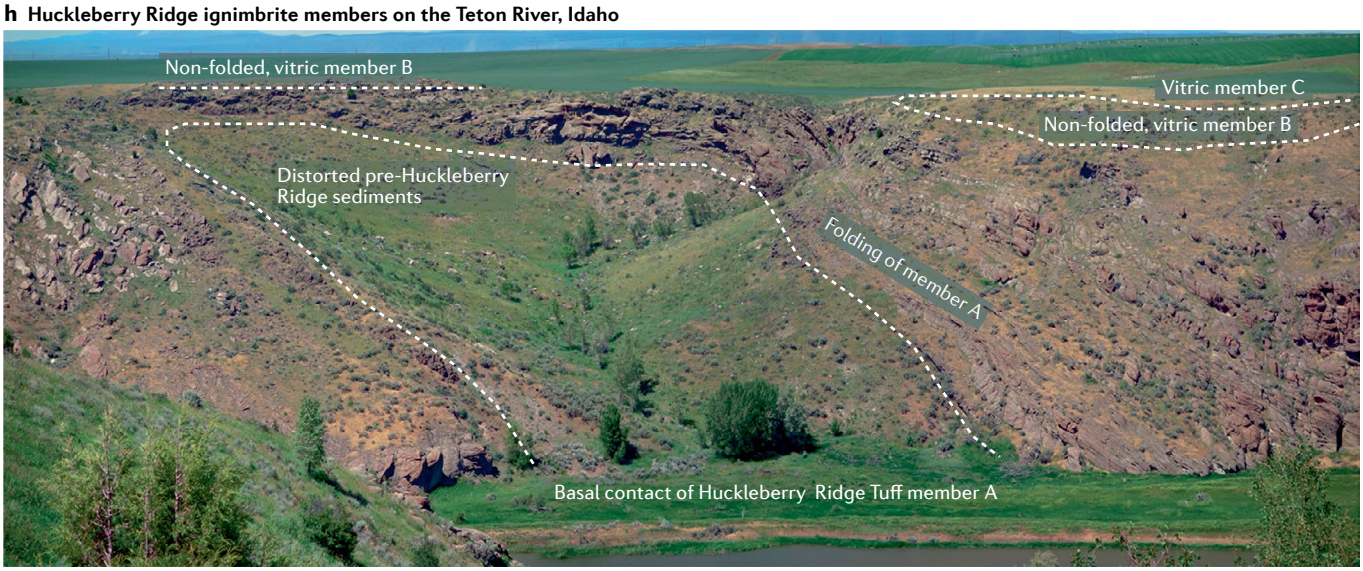

◀ Fig. 2 | **Field and textural relationships in supereruption deposits as guides to eruption characteristics.** Panels **a**–**c** show the spectrum of textural characteristics of ignimbrites, illustrating the types of materials present (juvenile and lithic) and the effects of welding due to high emplacement temperatures. Panels **d**–**h** show how characteristics of the boundaries between ignimbrite and/or fall units can indicate the relative time sequences of eruptions, for example, either no time break (**d**,**e**) or a distinct time break or prolonged deposition (**f**–**h**). **a** | Non-welded Bishop ignimbrite (Glass Mountain, California), with individual pumices (sampled for analysis) and lithics set in an ash matrix[24]. **b** | Incipiently welded Ongatiti ignimbrite[55] (near Hamilton, New Zealand), showing two kinds of silicic pumice (pumice 1, pumice 2), juvenile mafic and lithic clasts. **c** | Strongly welded Bishop ignimbrite (Aeolian Buttes, California), with the pumices flattened into black glassy fiamme[53], making them hard to sample. **d** | A thin wedge of non-welded Bishop ignimbrite[51] (Ig1Eb) enclosed in fall material at Chalfant, California, that can be demonstrated from the consistent influx of distinctive Glass Mountain rhyolite lava[36] lithics to be equivalent to and coevally emplaced with >70 m of densely welded ignimbrite ~15 km away (shown in panel **e**). **e** | >120-m-Thick densely welded Bishop ignimbrite in Owens Gorge, California. The density (equivalent to degree of welding) minimum does not occur at a horizon of any stratigraphic significance and cannot be associated with a prolonged time break[52], as the coeval fall deposits were continuously emplaced[51]. **f** | Early fall deposits of the Oruanui eruption near Taihape, New Zealand, showing the reworking (time break) between fall units 1 and 2 (REF.[57]). **g** | Early fall deposits of the Huckleberry Ridge eruption at Mount Everts, Wyoming, showing ripple bedding indicating wind reworking and prolonged deposition[59,60]. **h** | Field evidence for time breaks during the emplacement of ignimbrite members in the Huckleberry Ridge Tuff[26] in the gorge of the Teton River, Idaho. Height of exposure from valley floor to the top of the ridge is 80 m.

deposited coevally with the ignimbrites[37–39]) are rapidly quenched against the surrounding air, meaning that they preserve largely unaltered glass compositions[40–43]. These deposits are dominated by ash-sized shards and loose crystals, which, when coupled with their layer-by-layer deposition, can yield an unambiguous chronology of any compositional diversity or zonation within the original magmatic system[6,7,44].

Timing of individual eruptions. For individual explosive eruptions in general, a commonly held view based on historical examples is that the larger the event, the faster the eruption rate, and, hence, it has been suggested that supersized events might not last much longer than small events[3,45]. Some refer to even the largest events as occupying 'hours to days'[18], yet, there is often a lack of field evidence to constrain such conclusions. For example, studies of size grading in deep-sea ashes were used to suggest durations of days to weeks for the Youngest Toba, Indonesia, and Los Chocoyos, Guatemala[46,47], eruptions.

The relative timing of ignimbrite emplacement during an eruption can be constrained by observing if there are any direct links between fall deposition (that can be modelled through plume dynamics[48–50]) and coeval ignimbrite generation. In the case of the Bishop, the incoming of the Glass Mountain rhyolite lithics[36] are used to link fall deposits and ignimbrite (FIG. 2d,e) and demonstrate that they were coevally emplaced[51]. Using estimates of fall deposit deposition times, the Bishop eruption can then be inferred to have occupied roughly 1 week[24,51]. Longer durations (months to years) for the Bishop eruption were inferred from the presence of zones of lower welding intensity (rock density) in the ignimbrite that were assumed to represent periods of cooling[52], but such variations can be shown to have no chronological significance if temperatures of the emplaced materials were not uniform[53] (FIG. 2e).

Typically, the large-scale emplacement of ignimbrite and the onset of caldera collapse are widely inferred to be coeval[36]. As such, examples such as Youngest Toba[23,38], Whakamaru[54], Ongatiti[55] and Cerro Galán deposits[56], all of which lack initial fall deposits, are inferred to have begun abruptly, with collapse of the chamber roof occurring from the start of the eruption. Other supereruptions commenced with fall deposits vented from single or multiple vents. The transition into caldera collapse might then have occurred gradationally (Oruanui) or likely rapidly (Bishop, Tshirege, Otowi, Huckleberry Ridge), as the chamber roof began to collapse along ring fractures[36,51,57–59].

There is also a range of timings of eruptive phases within individual supereruptions. Some, like the Bishop, Youngest Toba and Cerro Galán, show no evidence in their deposits for substantial time breaks, whereas others show evidence for spasmodic activity. For instance, the first fall unit of the Oruanui eruption was deposited, then enough time elapsed (some months[57]) for the distinctive white ash to be reworked by burrowing animals before fall unit 2 was emplaced (FIG. 2f). Subsequent activity also included three pauses long enough for the eruption plume to dissipate and minor erosion to occur[57].

Early activity of the Huckleberry Ridge eruption occupied some weeks on the basis of wind reworking of the initial fall deposits[60] (FIG. 2g). This activity was followed by three ignimbrite members (A–C) being emplaced without hiatuses internally, but with their mutual contacts showing evidence of time breaks (FIG. 2h). In particular, along the Teton River gorge near Newdale, Idaho, member A was emplaced over a weak substrate that deformed under the load, distorting the welding fabric in the ignimbrite into domical folds cored by the remobilized underlying sediments. There was enough timing for this process to occur and the top surface of member A to partially cool, such that member B was chilled against it and is not deformed, suggesting a break of weeks to months. Members A and B together then had largely cooled in this area before member C was emplaced and was chilled against the underlying material to deposit vitric (glassy) material, suggesting a break of years to a few decades[26]. In most of the examples we consider here, however, this level of detail has not yet been determined, or is very challenging to interpret from the limited exposures available (for example, at Toba).

Bracketing eruptive events. Preceding and/or subsequent volcanic activity can supply information on the state of the magmatic system before and after the main supereruptive event. However, evidence of any preceding activity (particularly of lava domes) is sometimes destroyed during caldera collapse. For example, thousands to ten thousand years prior to the main climactic event, the Huckleberry Ridge system had a precursor lava dome[18]. There were also multiple explosive and effusive eruptions before the Oruanui, Lava Creek and Otowi eruptions[18,21,61,62]. All the other supereruptions we consider had no preserved precursors.

Subsequent eruptive events that follow the climactic supereruption represent the recovery time of the magmatic system and these are more commonly preserved in the geological record. Hence, in this Review, we are able

Juvenile material
Material that is newly discharged at the Earth's surface in an eruption.

Lithic material
Pre-existing (country) rocks caught up as fragments in the deposits of explosive eruptions.

Table 1 | **Quaternary supereruptive events and their summary features**

Eruption, volcano, country	Eruption age (ka)	Approx. volume of magma erupted (km^3)	Tectonic setting	Thickness of crust (km)	Number of silicic magmas tapped	Petrological estimates of minimum storage depth (km)	Magma temperature (°C)	Silica range of erupted magmas (wt%)	State of the magma body at time of eruption	Early fall deposits (with no ignimbrite)?	Time break(s) within the eruption?	Refs
Oruanui, Taupō, New Zealand	25.4	530	Subduction and rifting	15	Single homogenous with foreign intrusion	4–8	790–840	73–77 *(53–63)*	Cooling	Yes	Yes	25,57,61,74, 114,130,183
Youngest Toba Tuff, Toba, Indonesia	74	>2,800	Subduction and strike-slip	30–40	Multiple, zoned	3–6?	700–780	69–78	Cooling	No	No	23,38,42, 43,46,112, 121,132,189
Los Chocoyos, Atitlán, Guatemala	75	730	Subduction	40–50	Single(?), zoned or multiple(?)	Not determined	800–950	70–78	Not determined	Yes	No	39,47,190
Aso-4, Aso, Japan	86	>600	Subduction and rifting	30–35	Single, zoned	8–15	810–910	66–71 *(50–56)*	Mixing	No	Yes	28,191,192
Whakamaru, Whakamaru, New Zealand	350	>1,500	Subduction and rifting	15–25	Multiple	<6	720–820	70–77 *(53)*	Warming	No	No	42,54,70, 100,122
Lava Creek, Yellowstone, USA	631	1,000	Hotspot	48	Uncertain	3–10	820–880	74–77	Recharging	No?	Yes	18,37,62, 101,102,193
Bishop, Long Valley, USA	765	>600	Rifting	30–40	Single, zoned	4–8	700–840	73–78 *(57–72)*	Recharging	Yes	No	24,36,51–53, 75,105,106, 113–116,134, 183,194,195
Kidnappers, Mangakino, New Zealand	1,000	1,200	Subduction and rifting	15–25	Three	4–5.5	770–840	71–77	Cooling	Yes	No	44,64,97,128
Ongatiti, Mangakino, New Zealand	1,210	500	Subduction and rifting	15–25	Single, homogenous	4–6	770–840	66–73	Warming	No	No	55,128
Tshirege (Bandelier), Valles, USA	1,240	>400	Rifting	<30	Single, zoned	5–6	650–900	70–76	Recharging	Yes	No	27,58,95, 99,196
Otowi (Bandelier), Valles, USA	1,610	<550	Rifting	<30	Single, zoned	5–6	700–880	76–78	Recharging	Yes	No	58,68,95, 104,196
Cerro Galán, Cerro Galán, Argentina	2,080	630	Subduction	55–60	Single?, zoned	4–8	790–820	68–71	Recharging	No	No	56,96,131
Huckleberry Ridge, Yellowstone, USA	2,080	2,500	Hotspot	48	Multiple	4–8	800–950	66–78 *(50–66)*	Cooling	Yes	Yes	18,26,37, 59,60, 102,114, 129,183

Not included here is the Oldest Toba Tuff[23], as very little information is known about it. The Tshirege member of the Bandelier Tuff[58] is included as its volume approaches or might exceed the supereruption threshold. The silica range of erupted magmas indicates those of the main body or bodies tapped during the eruption, and, where present, the additional ranges in brackets are of minor, less evolved components.

to more thoroughly evaluate the larger dataset of subsequent activity. For instance, the first eruptions after the Youngest Toba event were effusive, occurring 5–15 kyr later[63], post-Oruanui explosive activity came about 5 kyr later[19] and Bishop effusive activity came no more than ~17 kyr later[20]. The magmas erupted after these short time breaks (from decades to ~5–20 kyr) generally show evidence for magmatic rejuvenation, sometimes in the form of hotter, crystal-poor rhyolite (for example, after the Bishop[20]) or as dacitic material that compositionally resembles the feedstock magma for subsequent rhyolite generation (for example, after the Oruanui[19]). An extreme short-timescale case is the Mangakino magmatic system in New Zealand, which evacuated a compositionally similar large (200-km^3) ignimbrite (Rocky Hill) only decades after the Kidnappers supereruption[64].

In contrast, there are substantially longer gaps (100–200 kyr) in the eruptive record at Yellowstone between the Huckleberry Ridge and Lava Creek eruptions and their respective oldest known younger (effusive) events[18]. Magmas erupted after these longer time breaks (like at Yellowstone[18,65,66]) are of comparable composition to the main events and it appears that the longer dormancy period allows for a fuller recovery of the magmatic system to rhyolitic eruptive compositions. In all cases, however, the whole crustal-scale magmatic system undergoes change after the supereruptive event, with evidence for renewed influxes of deeper seated, less evolved magmas and assimilation of existing mush and country rocks around the magma reservoir[19,20,67].

Cyclic activity of caldera systems. There is a wide spectrum of longer-term behaviour (that is, over tens to hundreds of thousands of years) within the eruptive sources of the Quaternary examples of supereruptions considered here (TABLE 1; FIG. 1). At one extreme, the Bishop[22], Cerro Galán[56] and Los Chocoyos[39] supereruptions represent, by far, the largest volume events at their respective volcanic centres and there were no other eruptions of a size large enough (typically over ~10 km^3) to induce caldera collapse. In contrast, the Valles[58,68], Yellowstone[18] and Toba[23] centres have each seen two supereruptions, plus at least one additional eruption large enough to generate caldera collapse in the last two cases. The Aso-4 eruption represents only the youngest (86 ka) and largest (>600 km^3) of four caldera-forming events focused within an 18 × 25 km area at that centre[28]. The four New Zealand examples (TABLE 1; FIG. 1) collectively are encompassed within a geographic area of similar size to the Yellowstone system (~120 × 60 km) but represent discrete multicycle foci of magma generation and eruption[69]. All four supereruptions were followed by additional, smaller but still caldera-forming eruptions: Kidnappers after only one to two decades[64], Whakamaru by about 10 kyr (REF.[70]), Oruanui by about 23.5 kyr (REF.[19]) and the Ongatiti by about 30 kyr (REF.[69]). In two of the New Zealand cases, the younger, smaller caldera-forming events discharged almost identical magmas (Kidnappers[55], Whakamaru[54]), whereas in the Oruanui example, the younger eruptions involve a magmatic system that generated contrasting compositions[19].

The controls on these complex relationships have not been fully explored, although models have been proposed to relate eruptive compositions and the growth of magmatic systems to sizes capable of caldera-forming (although not super-) eruptions[71,72]. However, there are demonstrable temporal variations in such key parameters as mafic magma supply rates into the system roots[22,30] and external tectonic controls in building and releasing large volumes of magma[25,60,73,74] that render generalized modelling problematic.

Supereruptive magmatic systems

Views on the nature of large silicic magmatic systems have changed over the last few decades from that of a unitary, long-lived, melt-dominated magma body to complex configurations of pre-eruptive magmatic generation and storage[11] (FIG. 3). These new views arise from five lines of evidence considered in the following subsections.

Long-term generation and mush storage. Silicic magmas are now widely inferred to be generated and stored over the long term (tens to hundreds of thousands of years) in vertically extensive, crystal-rich mush zones, rather than within large melt-dominant bodies, which are now thought to be short-lived features (centuries to thousands of years). Earlier models had the issue of how to separate crystals from melt to drive the fractionation processes[7,75]. The now widely adopted mush model reversed the process to separate the melt from the crystals, which is dynamically much easier[10,22,32,33]. Enhancements of the mush model consider the processes of reactivation and/or melt extraction from the mush and the relevant timescales involved[76–79]. However, the mush model is not universally accepted[80] because of disparities between modelled and actual trace element abundances in some ignimbrites, although alternative explanations for these disparities are now available[79,81].

The area of caldera collapse can provide an estimate of the areal extent of the evacuated portion of the magmatic system[82], but this approach can be misleading if there is peripheral slumping and/or lateral drainage of magma[57,83–85]. If the caldera area is divided by the erupted volume, the average vertical extent of the melt-dominant body or bodies can be estimated and, typically, is on the order 1–3 km (REF.[6]). These bodies can then be positioned in the crust using storage pressure estimates from melt inclusions or mineral geobarometry[86] or thermodynamic calculations of phase equilibria[87,88].

Mostly beneath (but also around) the melt-dominant bodies tapped during the eruption, there is the mush zone of intruded materials trending towards less evolved compositions (ultimately to the mantle-derived basaltic melts[30]). This deeper zone has long been recognized[6,7] but is now commonly referred to as a 'trans-crustal magmatic system'[11]. The architecture of this column can only be inferred for Quaternary systems[19,89,90], but from older examples where the crustal cross section has been exposed, these magmatic systems are compositionally zoned overall with complex internal geometries[91–93]. Processes in deeper parts of these systems, where intermediate composition magmas (andesites or dacites) are generated, are inferred from surface erupted compositions[22,94,95] and considered from numerical modelling[8,9]. A large degree of magmatic differentiation (from basalt to andesite or dacite) occurs within these lower crustal regions, prior to the establishment of pre-eruptive melt-dominant magma bodies[8]. However, the petrological record from these lower crustal regions is limited by the fact that the majority of the crystal cargo will remain in lower crustal mushy material or is diluted by later crystals formed in the midcrust to upper crust from the much larger volumes of more differentiated melt.

Through the identification of distinct crystal textures and populations in erupted products, it is possible, in some cases, to identify the relative extent of crystal growth within both the crystal-rich mush and the melt-dominated regions of the magmatic system[25].

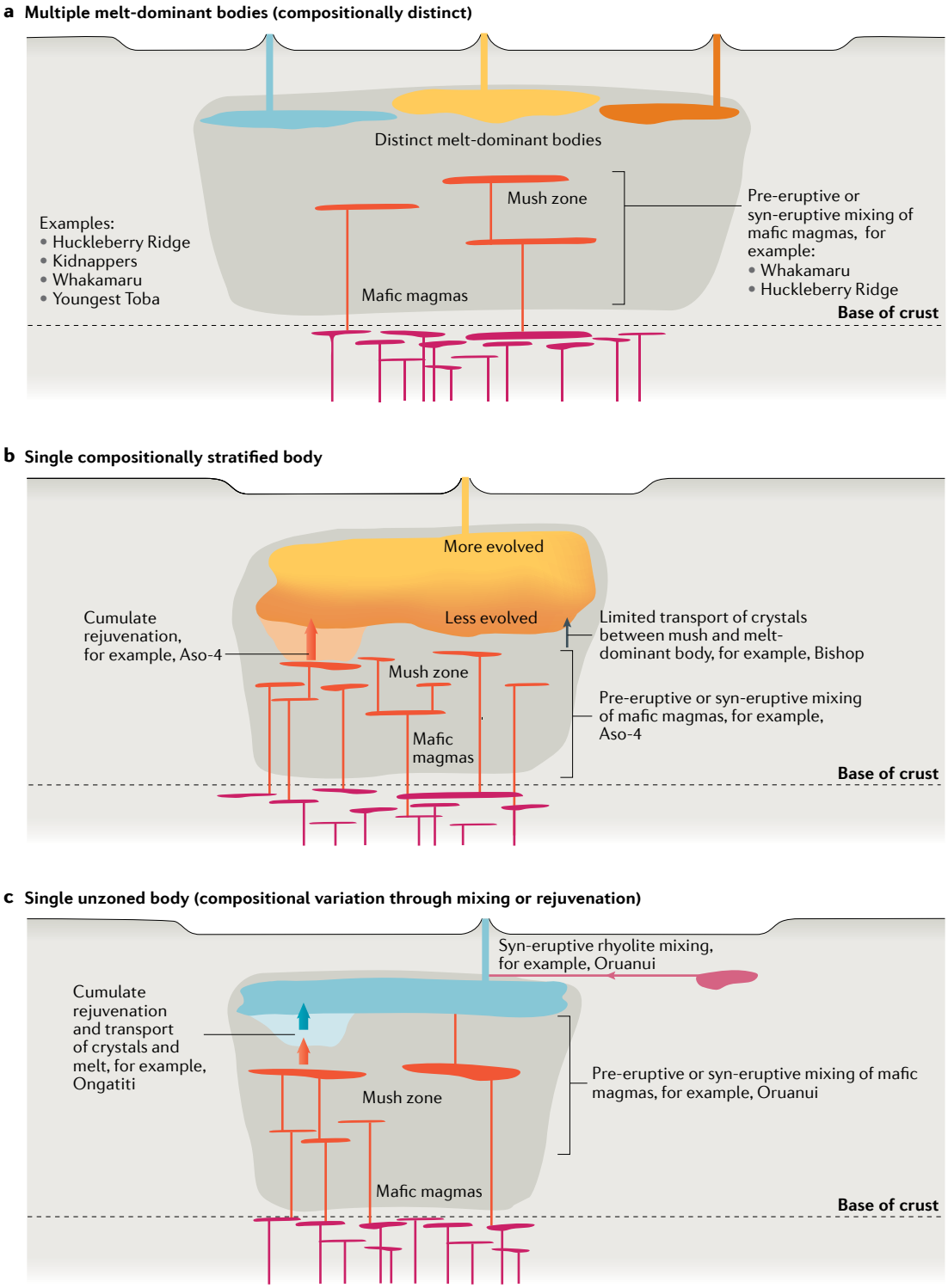

Fig. 3 | **Endmember pre-eruptive magmatic storage configurations for Quaternary supereruptions.** All three examples can be considered as trans-crustal magmatic systems, with mafic magmas intruding the lower crust and extensive, deep mush zones[6–8,11,12]. **a** | Multiple melt-dominant bodies that could be sequentially or simultaneously tapped during the eruption. Each body can be compositionally distinct, have unique crystal cargoes and be either homogenous or zoned. **b** | Single, compositionally stratified melt-dominant body. Compositional stratification (crystal content, melt composition) of the body is reflected within the deposits. **c** | Single unzoned melt-dominant body, with compositional variations arising through pre-eruptive or syn-eruptive mixing of other magmas (mostly more mafic than the main evolved storage body) or rejuvenation and melting of underlying cumulates (mush) by hot mafic magmas. Quaternary examples of supereruptions for each type of system and process are given where inferred from detailed petrological and geochemical studies (see TABLE 1 for references). These configurations represent endmember examples, and processes such as magma mixing and mush rejuvenation are not limited to the examples shown. The configuration of other examples discussed in the text (Lava Creek and Cerro Galán) are yet to be fully established, and, so, are not shown here.

Variations in melt–mush interaction have been inferred to take the form of one of the following: mush remobilization and eruption of crystal-rich magma; remobilization and rapid extraction of melts from a mush source; or melt extraction from a melt-dominant body (FIG. 3).

Mush remobilization and wholesale eruption of the remobilized mush (plus any separate melt-dominant bodies) produces crystal-rich (25–30 wt%) rhyolitic (for example, Ongatiti[55]) or less evolved deposits (for example, Cerro Galán[96] with 35–55 wt% crystals). At one extreme (not seen in Quaternary supereruptions), this mush remobilization generates very-crystal-rich dacitic ignimbrites, which are commonly labelled as 'monotonous intermediates'[7]. Mobilization of melt and crystals from the mush are often inferred to require 'defrosting' by an input of heat and/or volatiles[10,76–79].

Remobilization and rapid extraction of melts (plus entrained crystals) from an underlying source mush typically produces crystal-poor (<25 wt%) rhyolitic magmas that are sometimes not zoned in the chamber[32,79,97–102]. At an extreme, in the Oruanui, the melt-dominant body (with 3–13 wt% crystals) is inferred to have been generated rapidly in <600 years and mostly in <200 years[25] prior to the eruption. In addition, ~90% of the plagioclase and orthopyroxene crystal cores in the Oruanui high-silica rhyolite pumices are inherited from sources that span the entire compositional ranges of those crystals erupted in the whole 2-Myr history of the Taupō Volcanic Zone[25]. The root zones of the Oruanui system, thus, were complex, and the magma incorporated crystals that had grown in compositions ranging from mantle-derived basalts to rhyolites that were more evolved than those involved in the eruption itself, and also included recycled crystals from metasedimentary lithologies[103].

Transport of melt containing very few crystals from the mush zone into the melt-dominant magma body also typically produces crystal-poor (<25 wt%) zoned high-silica rhyolitic magmas, such as in the Bishop[24], Tshirege[99] and Otowi[104] examples. Only a small fraction of crystals in the Bishop Tuff, for example, can be linked back to the underlying mush: most appear to have grown in the melts in which they were erupted[24,105] and accumulation of the melt-dominant body is inferred to have been prolonged and piecemeal over tens of thousands of years[24,106].

The thermal (hence, physical) state of these mush systems remains a subject of controversy. There is an apparent disparity between the long-term (tens to hundreds of thousands of years) records for mush systems and the short-term (decades to millennia) records from diffusion studies in crystals[107]. From this disparity, it has been proposed that the mush is in a 'cold storage' state close to or below the solidus (<~650–700 °C for rhyolitic compositions) for most of its history[107,108]. In this state, diffusive processes are effectively arrested and melts and crystals are remobilized and extracted only shortly before eruption[107,108]. However, this model requires unusual thermal circumstances, for example, once the volatiles are lost from the system as it approaches the solidus, the reheating process has to reach the relevant dry solidus temperature in order to remobilize the crystal mush. This temperature is much higher than the magmatic temperatures of the erupted products and would profoundly affect the record in the crystals by causing dissolution of parts of the crystals and growth of new material with different (higher temperature) compositions.

The disparities in timescales from the crystal records used to propose cold storage remain an issue that requires explanation. As an alternative, 'warm storage' has also been proposed, where the long-term state of the mush entails that up to a few tens of percent melt be present[109]. This percentage of melt is enough to maintain some crystal growth, but, overall, the mush is too crystal-rich (>50–60 volume percent[110]) to readily erupt without an additional process such as melt separation or remobilization coming into play. Geophysical evidence beneath several modern silicic systems (for example, at Toba[90]; Yellowstone[89]; Laguna del Maule, Chile[111]) show the presence of modest amounts of melt (5–15 volume %), more consistent with the warm storage concept.

Conditions of shallow magma storage. There are three aspects of the shallow magmatic system during the generation and storage of eruptible, silicic melt-dominant bodies that are considered here because of their importance in understanding the diversity of supereruption magmatic systems. The first aspect concerns the number of pre-eruptive magma bodies. In contrast to the long held view of single bodies feeding the entire eruption (driven by the Bishop Tuff example[7,24]; FIG. 3), improved geochemical data coupled with more detailed field studies and sampling have frequently indicated the presence of compositional clustering, particularly for the largest examples considered here (for example, Youngest Toba[43,112] and Huckleberry Ridge[26,59,60]). Compositional clustering points towards the simultaneous and/or sequential tapping of multiple separate melt-dominant magma bodies[26,43,44,60,112] that show a spectrum of behaviour (FIG. 3).

The Kidnappers[44,97], Whakamaru[54], Youngest Toba[43,112] and Huckleberry Ridge[26,59,60] deposits were erupted from multiple separate magma bodies (FIG. 3a). In the Huckleberry Ridge case, not only were the melt-dominant bodies separate but also their root zones, whereby the whole eruption represents the evacuation of at least four separate magmatic systems[26,59,60]. In contrast, the magmatic systems feeding the Bishop, Ongatiti and Aso-4 eruptions appear to have come from single bodies[24,28,55] (FIG. 3b). For Oruanui, a single large body was invaded by a foreign, unrelated, silicic magma during the early stages of its eruption[25,74] (FIG. 3c). As the configuration of magma bodies at depth strongly interacts with (and is influenced by) the crustal stress field, discerning how many discrete magma bodies contribute to an eruption has important implications for long-term magma chamber stability and eruption-triggering mechanism(s)[13].

The second aspect concerns the nature and presence of compositional zonation within the magma body, where zonation can occur because of variations in the abundance of crystals (increasing downwards) or the composition of the melt phase (becoming less evolved downwards), or both (for example, Bishop[24,105]).

Although once considered to be ubiquitous[6,7], compositional variations in these large eruptions are not always present (TABLE 1), and can arise from a number of possible causes. Some systems show diversity in compositions, but these need not be systematically displayed in the eruptive ordering (for example, Oruanui[25]; Huckleberry Ridge[26]; Youngest Toba[112]). Other examples preserve a degree of orderly compositional stratification in the deposits that is linked to zonation in the magma body (Bishop[24]; Aso-4 (REF.[28])). The melting of earlier cumulate crystals (separated out from the melt in which they grew) and/or remobilization of mush material has been proposed as a means to account for geochemical and isotopic zonations preserved in large silicic deposits[79,81], and is seen in the extreme trace element variations in the Huckleberry Ridge system[25]. However, in other cases, the compositionally distinct melts contributing to the zonation appear to be less evolved precursors to the dominant more evolved magma[24,105]. Notably, those systems that record a signature of rapid melt extraction from the mush system (for example, Oruanui[25], Kidnappers[64,97]) lack evidence for compositional zonation within the melt-dominant magma bodies and appear to have been vigorously convecting when tapped by an eruption.

The third aspect concerns the depths and conditions for pre-eruptive magma storage. Although certain characteristics appear to be consistent between these voluminous eruptions, including the relatively narrow apparent range of pre-eruptive temperature (700–950 °C) and minimum storage depths (4–8 km; TABLE 1), these parameters represent transitory states of the magma reservoir and could be limited by the methods used to evaluate them (FIG. 4). Although crystal-specific studies provide records of the evolutionary history, these records are themselves limited to recording conditions where the relevant phase is stable. For example, our understanding of pressures, and, thus, depths, of storage are often determined by volatile (H_2O and CO_2) solubility relationships from quartz-hosted melt inclusions (for example, Bishop[113,114]). Quartz, however, will only stabilize late in the crystallization sequence, meaning that it lacks an older history and, thus, will only preserve the conditions associated with late-stage storage[115,116] (FIG. 4). Such limitations can be overcome through use of a broader range of mineral indicators[25,117]; however, this requires those minerals to be present in the crystallizing magma body. In addition, in the Oruanui, 90% of the plagioclase and orthopyroxene crystals in single pumices have cores that were inherited from older rocks[25]. Use of crystal abundances in eruption products to model the evolution of magmas towards a predicted state where eruption is triggered[118] is, thus, invalidated if the crystals are inherited. Some systems are more suited to a full reconstruction of intensive parameters because of the availability of large pumice clasts that have experienced limited post-depositional alteration and were rapidly quenched upon eruption (for example, Bishop, Oruanui). For those systems where these criteria are not met (for example, Lava Creek[18]), our current understanding of magma storage conditions are more severely limited.

Integrating these petrological models for the number, zonation, temperature and depth of magmatic storage regions highlights that the magma reservoirs feeding large silicic eruptions are architecturally diverse[12,82,119]. Yet, there is a tendency to classify storage regions into either being more 'tank-like' (single large body) or 'dispersed' (multiple smaller bodies)[120]. For instance, based on the modelled pressure ranges of the storage volume versus the caldera collapse area, the Oruanui, Bishop and Toba systems are considered 'tank-like', whereas the Huckleberry Ridge system is considered more 'dispersed'[120]. However, variably available data limit the application of this approach (particularly in the case of the Huckleberry Ridge[26]) and, to a first order, the configuration tells us little about what came next. For example, two 'tank-like' systems[120], Bishop and Oruanui, show overlapping model storage pressures and temperatures, yet, the Bishop 'tank' preserved an internal zonation (thermal and volatile[24,105,112,113]) and erupted rapidly and continuously, whereas the Oruanui 'tank' was remarkably well stirred and the eruption was spasmodic[25,57,74].

A diversity of timescales. The body or bodies of melt-dominant magma that lead to eruption can accumulate over a range of timescales, from tens of thousands of years down to centuries[24,64,106,117,121,122]. Development of the overall magma system can be quantified through radiometric age-dating of preceding eruptions, which, ultimately, shows that the activity associated with supereruptions might date back hundreds of thousands of years[22,95], but can be as short as a few tens of thousands of years[61]. These timescales highlight a contrast between the longer-term history of the magmatic system, during which processes of mafic influx, assimilation (of country rocks or earlier crystallized products of the system) and fractionation occur, versus the shorter timescales for physical assembly of eruptible magma bodies. Assessment of the magmatic histories preserved in eruption products involves two methods that yield complementary perspectives. The first is U–Pb or U–Th techniques used to date crystallization ages of U-rich and/or Th-rich accessory phases that are commonly present in the rhyolites that form the dominant volume of melts tapped in supereruptions (BOX 1). The second is diffusion geochronometry, which assesses the relative timing of formation of a compositional boundary through the consequent time-dependent diffusive relaxation of this boundary within crystals. These boundaries and extracted timescales can be linked to specific processes through detailed petrological study.

Absolute age dating of accessory phases (principally zircon, but also other U-bearing and Th-bearing accessory phases[123–125]) has shown that records of large silicic volcanic systems are relatively short (tens to hundreds of thousands of years) when compared with their older plutonic counterparts that typically record zircon crystallization timescales spanning millions of years[5,126,127]. Among the extensive literature of zircon age data, there is a diversity in the age spectra preserved within supereruption deposits. Unimodal age spectra, with minimal or no recycling of zircons from previous magmatic events, are seen in the Bishop[106], Ongatiti[128] and Huckleberry Ridge[102,129] deposits. These spectra reflect mush systems with zircon formed early in the

Cumulate
Crystals grown in the mush that have been separated out from the melt in which they grew and, hence, can generate contrasting compositions of melt if reheated.

Absolute age
An age determined by measurements of radioactive decay in minerals and associated with the time period since closure of the system.

Zircon
Used to determine age (U–Pb, U–Th) and then infer residence time within magmatic systems. Trace elements can also record long-term evolution processes.

Fe–Ti oxides
Compositional data between two pairs is often used to extract temperature information. Zoning can inform on short timescales.

Pyroxene
Used for unravelling timescales of mixing between changing external conditions, based on diffusive gradients. Spot analysis can be used in geothermobarometers.

Amphibole
Determine temperature and/or pressure and melt chemistry during crystallization.

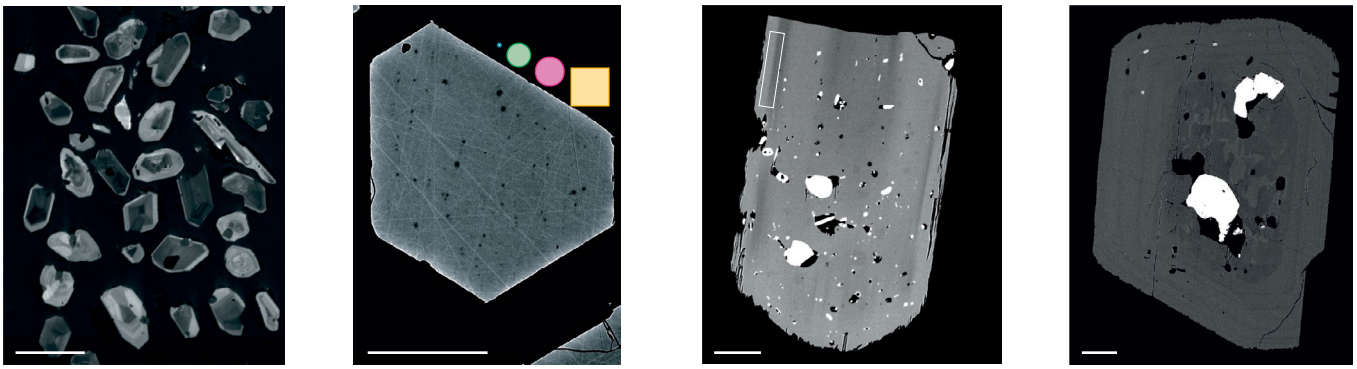

Earlier crystallization and/or longer residence time

Plagioclase
Zoning can be used to extract compositional evolution of the melt through individual spot analysis, which includes estimating the H_2O content of the crystallizing melt. Some plagioclase crystals, however, are inherited (right), meaning that they record an older history.

Sanidine
Used for Ar–Ar age dating on the later stages of magma accumulation. Also can apply diffusion modelling to any rims.

Quartz
Used for pressure restoration through H_2O and CO_2 measurement in melt inclusions, timescales of mixing based on growth zones, sometimes temperature based on Ti in quartz.

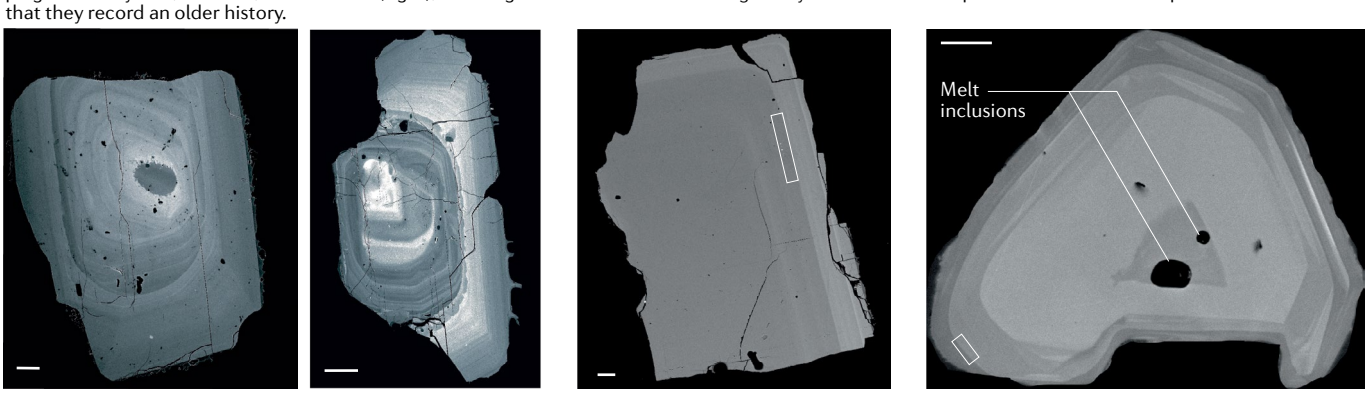

Later crystallization - records later processes

○ Spot analysis by EPMA, SIMS, LA-ICP-MS or FTIR ▯ Diffusional boundary used for modelling timescales

Fig. 4 | **The mineral toolbox for probing the origins and evolution of silicic magmatic systems.** The mineral phases commonly found in silicic magmas are shown, with indications of their main use in unravelling the pressure, temperature and compositional evolution of their respective magmas, or, additionally, the associated timescales of magma accumulation and eruption. Cathodoluminescence (zircon, quartz) and backscattered electron (all other mineral phases) images from scanning electron microscopy are shown for a selection of mineral phases. The white scale bar in all images is equal to 100 microns. White open boxes indicate examples of compositional changes where diffusion modelling can be applied across the compositional variations represented by the grey tonality. Representative spot sizes are shown in the Fe–Ti oxides panel for: electron probe microanalysis (EPMA: blue), secondary ion mass spectrometry (SIMS: green), laser ablation inductively coupled plasma mass spectrometry (LA-ICP-MS: pink) and Fourier-transform infrared spectroscopy (FTIR: yellow).

geochemical evolution of these bodies, and then continuing to crystallize. In contrast, zircon age spectra from the Oruanui[61,130], Kidnappers[128], Cerro Galán[131] and Youngest Toba[132] deposits all have multiple peaks, indicating episodic growth or recycling of earlier magmatic systems. The lack of recycled zircons within systems like Bishop and Huckleberry Ridge suggests that, rather than supersizing a pre-existing magmatic system[6,133], any earlier magmatic systems are effectively reset. This interpretation would imply that the supereruptive events required a strong change in storage conditions, such as thermal resetting of the system[22]. On the basis of the zircon and other age data, it is apparent that large silicic magmatic systems do not accumulate and crystallize on any special timescale, and that the amount of magma eventually erupted is not simply related to the time over which the mush system or its melt-dominant bodies have been extant.

In contrast to absolute age dating, relative age timescales inferred from diffusion studies are typically more focused on shorter-lived processes, typically <1 kyr. However, relative ages that can be measured

Relative age
An age that is determined, typically through measurements of diffusion profiles in minerals, relative to the point of quenching by eruption.

Box 1 | **Dating accessory phases for magmatic histories**

For the purpose of following the growth and development of the magmatic systems that feed silicic eruptions, accessory phases (such as zircon or allanite) lend themselves to radiogenic absolute age dating. The methods primarily use the U and/or Th decay series, as these minerals preferentially include U and Th and exclude Pb during crystal growth[123–125]. Subsequent changes through reequilibration are inhibited by the exceptionally slow diffusion rates of Pb through the mineral structure and, so, pre-eruptive ages of crystal growth remain undisturbed[197]. Various methods can be used to date these phases, each with their own advantages and limitations. There is a trade-off between the precision of an age determination and the volume of material consumed, such that ultra-high precisions can normally only be obtained as average ages from whole crystals. Thus, the method employed to date accessory phases largely depends on the process(es) of interest:

1. Cross-sectional in situ analysis of polished grains using secondary ion mass spectrometry (with an ion probe[125,198,199]) or laser ablation inductively coupled plasma mass spectrometry[200,201] can be used to give analyses of core, intermediary and near-rim domains within single crystals. Combining many analyses can reveal inheritance and punctuated growth of these accessory phases. Uncertainties on individual analyses are high and these can only be reduced by compiling many tens to hundreds of analyses. Estimates of eruption age within uncertainty of $^{40}Ar/^{39}Ar$ eruption ages can be obtained in favourable cases[106].
2. Surface profiling by in situ analysis of unpolished grain surfaces can be used to date the latest stage of mineral growth, and has also been shown to yield ages within uncertainty of $^{40}Ar/^{39}Ar$ eruption ages[193]. Individually, these age determinations are relatively imprecise, owing to high analytical uncertainty, although multiple age determinations can be combined. In addition, the evolutionary history of the magma bodies as reflected in crystal growth is not recovered with this method.
3. Chemical dissolution of individual zircon grains for analysis by isotope dilution thermal ionization mass spectrometry yields highly precise ages (with analytical precision similar to that of $^{40}Ar/^{39}Ar$ methods[102,129,194]), but this gives an averaged age for the entire mineral grain and obscures any growth history or inheritance.

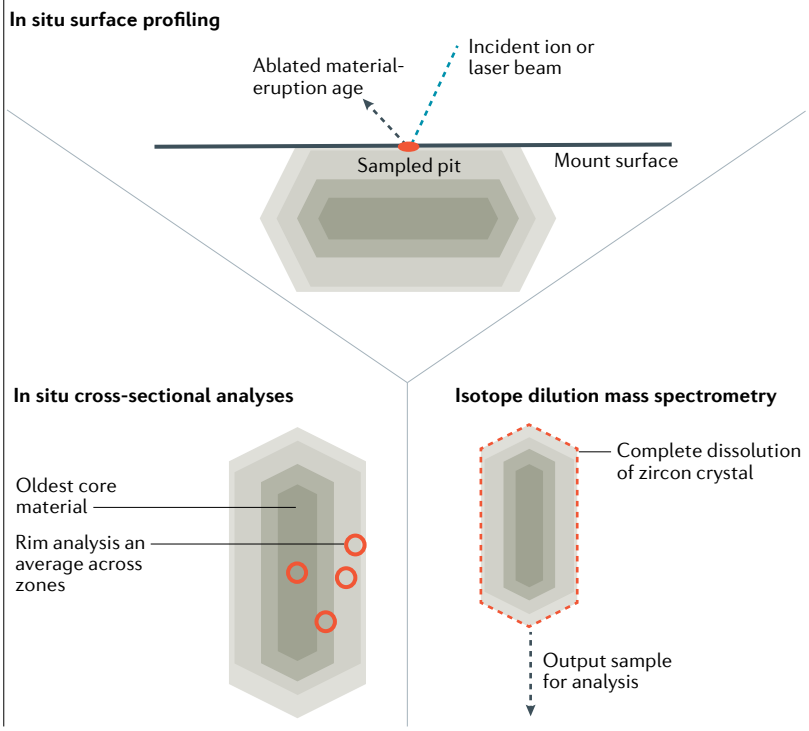

are dependent upon the mineral and element systems utilized and the applicable temperatures[134,135]. These studies consider processes such as the extraction of melt from the mush and its accumulation into eruptible, melt-dominated bodies[25,64,117], or the disturbance, for example, by mafic mixing into a crystallizing silicic magma body, eventually leading to eruption[100,101,134]. These timescales are commonly based on modelling the relaxation of an originally sharp compositional boundary within mineral phases using diffusion chronometric techniques[135]. Such boundaries are inferred to be generated by the changes in growth conditions accompanying the disturbance of the mush or transport of the crystal between the mush and melt-dominant body. Diffusion-based timescales require an original step boundary to be approximated within the crystal, where distinguishing between profiles generated by diffusive relaxation versus mineral growth can be problematic[135]. In some large silicic systems, the timescales of destabilization and/or accumulation appear to be on the order of decades to centuries prior to eruption, despite the large size of the magma bodies[25,101]. Such short timescales appear to apply also to smaller-scale caldera-forming eruptions of silicic magmas[64,98,136], implying that a common suite of processes can be involved. Other large examples, like the Bishop and Youngest Toba, show evidence for more gradual changes approaching the climactic outburst[132,134].

Structural controls on location and eruption dynamics. The locations of large silicic systems in the Quaternary can be linked, in general, to tectonic setting[137]. In addition, although a range of numerical models are available that propose why and when these large eruptions occur when they do, many of these models treat the melt-dominant body as a system isolated from the external stress field, then propose singular causes for eruption triggering[13–17,138]. However, there is increasing evidence for the role of external tectonic forces in controlling both the location of magmatic systems and the dynamics of magma accumulation and release[16,60,74].

The locations of most systems considered here are in convergent margin settings, areas of extension and/or strike-slip tectonics (particularly in the case of Toba[139]) (TABLE 1). The Bishop deposits were vented from the largest of a series of magmatic systems, active over several million years, erupting from a transtensional region at the juncture of the Sierra Nevada microplate and the extensional Basin and Range Province[22,73]. For the four Quaternary supereruptions in New Zealand, the interplay between volcanism, magmatism and the rift architecture has strongly influenced the position of large-scale caldera collapses[140], with caldera–tectonic linkages inferred in large eruptions[85]. Similar considerations also apply to some smaller but active silicic systems, such as Santorini, Greece[141] and Laguna del Maule, Chile[142].

There are also several lines of evidence for syn-eruptive tectonic controls on the dynamics of large eruptions. The simultaneous and sequential eruption of discrete magma bodies during the opening stages of the Huckleberry Ridge eruption is inferred to reflect vents becoming active through tectonic linkages[60]. In the case of the Oruanui event, concurrent rifting is inferred to have modulated the early stages of the eruption, as well as permitting the lateral 'invasion' of a foreign silicic magma from an adjacent, unrelated system into

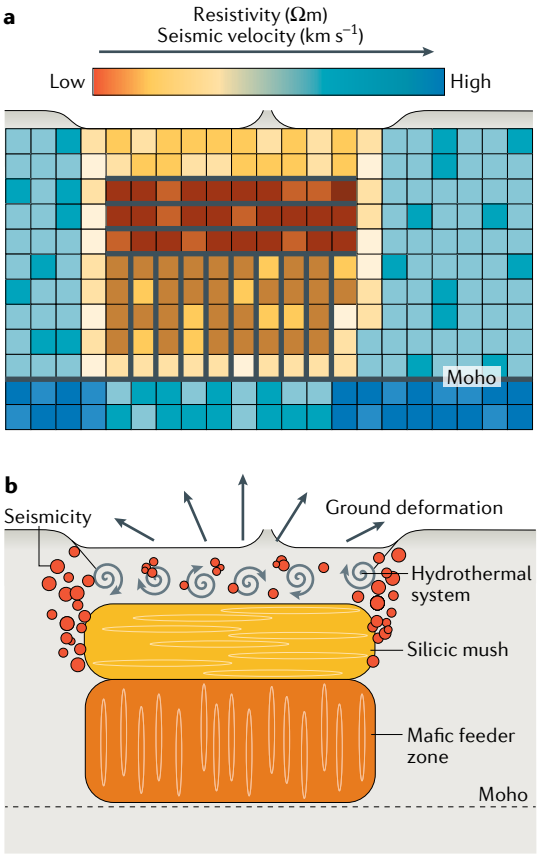

Fig. 5 | **Geophysical imaging of supereruptive systems.** Geophysical resolution is typically on the order of 5–10 km and is not sufficient to image localized melt bodies[147–149]. However, these methods have revealed that modern magmatic systems have a stratified structure that is broadly consistent with constraints from petrological studies. **a** | A schematic cross-sectional view of a supereruptive magmatic system as imaged by geophysical methods, such as magnetotellurics and seismology. The cell size is indicative of the degree of spatial resolution. The silicic mush (see panel **b**) is dominated by horizontal structures (for example, sills, shown as horizontal black lines) and the less evolved feeder zone is dominated by vertical structures (for example, dykes, shown as vertical black lines)[90,139,154–156]. The crustal thickness (depth to the Moho) can be between 15 and 60 km, depending on the local setting for each volcano (TABLE 1). **b** | Monitoring of supereruptive and other centres relies on the detection of periods of unrest, often associated with heightened seismic activity (hypocentres shown as red filled circles), ground deformation (straight black arrows) and/or changes to the shallow hydrothermal system (grey spirals)[163,165–179]. However, the majority of unrest episodes do not lead to any eruption.

the supersized Oruanui body[74]. Caldera formation is, in itself, an extreme example of a tectonic event, and the shapes of the calderas associated with large eruptions often reflect the orientation of tectonic elements in the shallow crust[143]. For example, the shape and NW-SE elongation of the Oruanui structural caldera are coincident with a cross-arc soft linkage, whereas the Whakamaru caldera margin to the north (FIG. 1) is influenced by a behind-arc rift[140,144].

Geophysical studies of modern large silicic systems. Geophysical imaging techniques (FIG. 5a) can provide a snapshot in time of the location, size and state of contemporary large silicic magmatic systems and ongoing processes within them. Combining multiple geophysical techniques with geochemical and petrological data from past eruptions to constrain interpretations yields our best picture of the present-day state of large (supersized) magmatic systems, both quiescent and restless.

Although geophysical surveys demonstrate that some supereruptive systems have an active, partially molten magma reservoir, none of them show evidence for the large, shallow, melt-dominant bodies (tens to hundreds of cubic kilometres) that are inferred to feed supereruptions[89,139,145,146]. However, as melt-dominant bodies are thought to be ephemeral[11,12], it is possible that they are currently absent within these magmatic systems. Estimating melt percentages from geophysical signals is not straightforward[147,148] and, typically, tomographic results show only an averaged view of the subsurface structure[149]. The resolution is often limited to ~5–10 km (FIG. 5), reflecting the seismic wavelengths used in such studies and the typical station spacing of seismic networks. Therefore, geophysical imaging currently does not have the resolution to determine whether smaller (<10 km^3) melt-dominant bodies, which are still capable of producing eruptions[19,98], are present or not. Outstanding questions, therefore, remain around when these melt-dominant bodies begin to accumulate or crystallize back to mush, and what geophysical signals (if any) would be detected with current technology.

An ultimate goal is to use modern geophysical methods along with geological knowledge of past events to provide operationally useful forecasts around future unrest and eruptive activity; however, this goal often remains out of reach. Owing to its location and restless nature, Yellowstone is the most extensively geophysically studied supervolcano[150]. A large amount of effort at Yellowstone has been focused on seismically imaging the magma reservoir, through controlled source experiments[151], earthquake tomography[89,152–154] and ambient noise tomography[155,156]. When combined, these studies indicate that the Yellowstone volcanic system is underlain by a large silicic upper-crustal magma reservoir organized into stacked sills and an underlying basaltic lower-crustal magma reservoir (FIG. 5b). These reservoirs are crystal-rich, with the upper-crustal silicic reservoir containing 5–15% melt and the lower-crustal basaltic reservoir 1–2% melt[89,154]. However, the resolution of imagery cannot preclude modest-sized melt-dominant bodies (up to the 1–10 km^3 range) from being present at large silicic caldera systems[152,157], like at Yellowstone[89].

Many large silicic systems share common attributes with Yellowstone: vigorous hydrothermal systems in the near-surface that are fuelled by more evolved magma mush systems in the midcrust that are, in turn, underlain by a mafic feeder zone (FIG. 5b). Similar studies at Aso[158], Toba[90,139] and Taupō[145] also show evidence, through seismic, gravity and magnetotelluric surveys, that regions of partial melt presently reside beneath or close to these caldera systems. Long Valley is controversial: contrasting

geophysical and geological evidence is put forward to propose[146,159] or refute[160,161] the presence of magma beneath the caldera. These observations of regions of partial melt are in accord with the trans-crustal-scale architecture suggested by geochemical and petrological studies on volcanic products[7,10–12,19,25,26,95] and also with that observed in exhumed ancient examples[91–93]. Repeat and/or continuous geophysical surveys on active systems offer the opportunity to monitor any changes in modern magmatic systems.

Caldera volcanoes often undergo periods of elevated seismicity, ground deformation and gas emission, known as unrest (FIG. 5). An important point is that unrest events do not imminently indicate an impending eruption and that eruptions come in all sizes, even at volcanoes that have hosted past supereruptions[18,22,162]. Although it is assumed that all eruptions from large silicic systems are preceded by some level of unrest, the vast majority of unrest periods are not followed by an eruption[163]. Monitoring systems at volcanoes worldwide commonly include seismic networks, ground deformation monitoring and surficial fluid emissions monitoring. For example, the Yellowstone Volcano Observatory issued a monitoring plan[164] in 2006 that stated that the system in place should detect signals that could indicate changes in Yellowstone's magmatic system, including earthquakes, ground deformation and/or increased heat, gas or water flux. However, such monitoring depends on the ability to distinguish between normal behaviour and some transient change in behaviour (unrest) that could be related to magmatic activity.

During the time that Yellowstone has been monitored, there have been numerous unrest episodes, including large seismic swarms[165–168] and episodes of accelerated ground deformation[169–171]. Similar but less vigorous unrest episodes have also been observed at supervolcanoes at Long Valley[172–174] and Taupō[175–177], as well as at other large silicic centres, such as Campi Flegrei[178,179] and Laguna del Maule[142,157]. However, none of these episodes has yet led to a volcanic eruption. Therefore, it is imperative that monitoring systems at large silicic volcanoes monitor for multiple signals (that is, seismic, deformation, gas release etc.), as a change in one signal likely does not point to an impending eruption, but simultaneous changes in all signals might point to the movement of magma into the shallow crust and the possibility of eruption.

Summary and future perspectives

Synthesis of field and petrological studies of supereruption products shows that there is great diversity in the nature of these events, making it challenging when considering the current behaviour of modern systems. Supereruptions can start literally with a bang and collapse of the chamber roof or begin gradually, with hesitancy before escalating into catastrophic activity. Overall, the eruption can be rapid, uninterrupted events over a few days or an episodic sequence prolonged over decades. Magmas that feed supereruptions can come from single or multiple final storage regions, which can be zoned or convectively mixed. Magmas are assembled into their eruptible states across diverse timescales, in extreme cases involving magmatic accumulation rates exceeding 1 km^3 per year. Our brief Review serves to emphasize three points about the present-day states of the large silicic systems that have produced Quaternary supersized or other large silicic eruptions.

First, non-eruptive unrest events at large silicic volcanoes are one to three orders of magnitude more common than the probability of unrest leading to an eruption of any size. Petrological studies have, however, highlighted that large silicic systems record timescales suggesting that extraction and accumulation of eruptible magma can occur over periods of only a few years. The ability of a silicic system to move into a state of eruptive capability so rapidly presents challenges in the modern instrumented era, and the factors (tipping points) that cause unrest associated with sufficient accumulation of magma to evolve into eruption remain unquantified[180]. Limited data on silicic magma accumulation rates suggest that, once the magma begins to ascend, the warning time for eruption onset could only be days to months, giving little time for interpretation of changing geophysical signals.

Second, further work to improve field-focused studies of eruption timings and products and integrate them with crystal-specific reconstructions of the magma bodies and numerical modelling remains to be done around understanding supereruptive magmatic systems. There is a marked contrast between the overall long lifetimes (hundreds of thousands to thousands of years) of large silicic systems versus intermediate timescales of eruptible magma accumulation (thousands to hundreds of years) versus the short timescales of triggering and eruption (decades to days). These contrasting timescales suggest either a remarkable uniformity of behaviour across systems of widely varying sizes or the presence of other unknown factors[180] that are currently overlooked. Evidence for the timing and nature of physical processes associated with eruptions is scant, yet, this evidence is important in assessing the nature of future activity and associated hazards. Numerical modelling of volcanic behaviours requires further development, including better understanding of the role of external factors such as tectonic forces and crustal stress states influencing magma accumulation, establishing the onset and modulation of eruptions and resolving the role of the hydrothermal envelope in causing geophysical unrest signals. In addition, current numerical modelling of melt extraction is still largely based on the formation of a single melt-dominant reservoir, without consideration for more complex configurations indicated from several petrological studies.

Third, supereruptions in the past define a supervolcano but do not dictate the modern behaviour of the volcano or help constrain the size of future activity. The common perception of a volcano such as Yellowstone is that any future event will be catastrophic[181], yet, this is most improbable. The question then arises whether non-eruptive unrest behaviour can be defined at these large silicic systems versus the signals related to an impending eruption. Since there have not been eruptions at large silicic caldera-forming systems in modern (instrumented) times, this question cannot be answered

definitively and there is much room for further work. Application of new tools such as machine learning algorithms[182] in monitoring systems at large silicic systems might be able to permit timely interpretation of transient signals that reflect the onset of movement of stored magma towards the surface on the hours-to-days timescales indicated from petrological studies[60,183]. In addition, laboratory experiments linking direct measurements of melt percentage and seismic velocity[184,185] will aid in the interpretation of tomographic results with respect to the amount of melt available in a magma reservoir. There is also a need to improve our understanding of non-eruptive unrest at caldera systems[163], as these events can cause major societal and economic impacts[175,186–188]. These impacts can be exacerbated by public perceptions of supervolcanoes as liable to catastrophically erupt (particularly Yellowstone[181]), whereas, in reality, such an event is extremely unlikely. Therefore, effective education and communication of the nature and frequency of unrest at large silicic systems is a key mitigation strategy against the societal impacts of future unrest episodes.

Published online: 27 July 2021

1. Mason, B. G., Pyle, D. M. & Oppenheimer, C. The size and frequency of the largest explosive eruptions on Earth. *Bull. Volcanol.* **66**, 735–748 (2004).
2. Sparks, R. et al. *Super-Eruptions: Global Effects and Future Threats. Report of a Geological Society of London Working Group* 1–24 (The Geological Society, 2005).
3. Self, S. The effects and consequences of very large explosive volcanic eruptions. *Philos. Trans. R. Soc. Lond. A* **364**, 2073–2097 (2006).
4. Wark, D. A. & Miller, C. F. (eds) Supervolcanoes. *Elements* **4**, 11–49 (2008).
For the non-specialist, still the single most useful collation of information about supersized eruptions and their source volcanoes.
5. Lundstrom, C. C. & Glazner, A. F. (eds) Enigmatic relationship between silicic volcanic and plutonic rocks. *Elements* **12**, 91–127.
6. Smith, R. L. Ash-flow magmatism. *Geol. Soc. Am. Spec. Pap.* **180**, 5–27 (1979).
7. Hildreth, W. Gradients in silicic magma chambers: implications for lithospheric magmatism. *J. Geophys. Res.* **86**, 10153–10192 (1981).
A classic comprehensive overview and synthesis of the nature of many types of magmatic systems (including supersized examples) that acted as a springboard for many subsequent studies.
8. Annen, C., Blundy, J. D. & Sparks, R. S. J. The genesis of intermediate and silicic magmas in deep crustal hot zones. *J. Petrol.* **47**, 505–539 (2006).
9. Annen, C. From plutons to magma chambers: thermal constraints on the accumulation of eruptible silicic magma in the upper crust. *Earth Planet. Sci. Lett.* **284**, 409–416 (2009).
10. Bachmann, O. & Huber, C. Silicic magma reservoirs in the Earth's crust. *Am. Mineral.* **101**, 2377–2404 (2016).
11. Cashman, K. V., Sparks, R. S. J. & Blundy, J. D. Vertically extensive and unstable magmatic systems: a unified view of igneous processes. *Science* **355**, eaag3055 (2017).
12. Sparks, R. S. J. et al. Formation and dynamics of magma reservoirs. *Philos. Trans. R. Soc. Lond. A* **377**, 2018.0019 (2019).
13. Gregg, P. M., de Silva, S. L., Grosfils, E. B. & Parmigiani, J. P. Catastrophic caldera-forming eruptions: thermomechanics and implications for eruption triggering and maximum caldera dimensions on Earth. *J. Volcanol. Geotherm. Res.* **241–242**, 1–12 (2012).
14. Degruyter, W. & Huber, C. A model for eruption frequency of upper crustal silicic magma chambers. *Earth Planet. Sci. Lett.* **403**, 117–130 (2014).
15. Karakas, O., Degruyter, W., Bachmann, O. & Dufek, J. Lifetime and size of shallow magma bodies controlled by crustal-scale magmatism. *Nat. Geosci.* **10**, 446–450 (2017).
16. Cabaniss, H. E., Gregg, P. M. & Grosfils, E. B. The role of tectonic stress in triggering large silicic caldera eruptions. *Geophys. Res. Lett.* **45**, 3889–3895 (2018).
17. Townsend, M. & Huber, C. A critical magma chamber size for volcanic eruptions. *Geology* **48**, 431–435 (2020).
18. Christiansen, R. L. The Quaternary and Pliocene Yellowstone Plateau volcanic field of Wyoming, Idaho, and Montana. *U.S. Geol. Surv. Prof. Pap.* **729-G**, 1–143 (2001).
19. Barker, S. J., Wilson, C. J. N., Allan, A. S. R. & Schipper, C. I. Fine-scale temporal recovery, reconstruction and evolution of a post-supereruption magmatic system: Taupo (New Zealand). *Contrib. Mineral. Petrol.* **170**, 5 (2015).
20. Hildreth, W., Fierstein, J. & Calvert, A. Early post-caldera rhyolite and structural resurgence at Long Valley caldera, California. *J. Volcanol. Geotherm. Res.* **335**, 1–34 (2017).
21. Troch, J. et al. Rhyolite generation prior to a Yellowstone supereruption: insights from the Island Park–Mount Jackson Rhyolite series. *J. Petrol.* **58**, 29–52 (2017).
22. Hildreth, W. Volcanological perspectives on Long Valley, Mammoth Mountain, and Mono Craters: several contiguous but discrete systems. *J. Volcanol. Geotherm. Res.* **136**, 169–198 (2004).
23. Chesner, C. A. The Toba caldera complex. *Quat. Int.* **258**, 5–18 (2012).
24. Hildreth, W. & Wilson, C. J. N. Compositional zoning of the Bishop Tuff. *J. Petrol.* **48**, 951–999 (2007).
25. Allan, A. S. R. et al. A cascade of magmatic events during the assembly and eruption of a super-sized magma body. *Contrib. Mineral. Petrol.* **172**, 49 (2017).
A comprehensive linking of physical volcanology with magmatic processes inferred from petrological data and magmatic timescales from multiple mineral phases to document the evolution of a supereruptive system.
26. Swallow, E. J., Wilson, C. J. N., Charlier, B. L. A. & Gamble, J. A. The Huckleberry Ridge Tuff, Yellowstone: evacuation of multiple magma systems in a complex episodic eruption. *J. Petrol.* **60**, 1371–1426 (2019).
27. Boro, J. R., Wolff, J. A. & Neill, O. K. Anatomy of a recharge magma: hornblende dacite pumice from the rhyolitic Tshirege Member of the Bandelier Tuff, Valles caldera, New Mexico, USA. *Contrib. Mineral. Petrol.* **175**, 96 (2020).
28. Kaneko, K., Kamata, H., Koyaguchi, T., Yoshikawa, M. & Furukawa, K. Repeated large-scale eruptions from a single compositionally stratified magma chamber: an example from Aso volcano, Southwest Japan. *J. Volcanol. Geotherm. Res.* **167**, 160–180 (2007).
29. de Silva, S. L. & Gosnold, W. A. Episodic construction of batholiths: insights from the spatiotemporal development of an ignimbrite flare-up. *J. Volcanol. Geotherm. Res.* **167**, 320–335 (2007).
30. Barker, S. J. et al. What lies beneath? Reconstructing the primitive magmas fueling voluminous silicic volcanism using olivine-hosted melt inclusions. *Geology* **48**, 504–508 (2020).
31. Gelman, S. E., Deering, C. D., Bachmann, O., Huber, C. & Gutiérrez, F. J. Identifying the crystal graveyards remaining after large silicic eruptions. *Earth Planet. Sci. Lett.* **403**, 299–306 (2014).
32. Bachmann, O. & Bergantz, G. W. On the origin of crystal-poor rhyolites: extracted from batholithic crystal mushes. *J. Petrol.* **45**, 1565–1582 (2004).
This paper marked a paradigm shift in how we view magmatic systems, providing an integrated model of mush zones and the evolution of the plutonic and volcanic components of the system.
33. Bachmann, O. & Bergantz, G. W. Rhyolites and their source mushes across tectonic settings. *J. Petrol.* **49**, 2277–2285 (2008).
34. Wilson, C. J. N. Supereruptions and supervolcanoes: processes and products. *Elements* **4**, 29–34 (2008).
35. Walker, G. P. L. Crystal concentration in ignimbrites. *Contrib. Mineral. Petrol.* **36**, 135–146 (1972).
36. Hildreth, W. & Mahood, G. A. Ring-fracture eruption of the Bishop Tuff. *Geol. Soc. Am. Bull.* **97**, 396–403 (1986).
Details a unique circumstance by which lithic clasts within a deposit are used to reconstruct the development of an iconic caldera-forming eruption.
37. Izett, G. A. & Wilcox, R. E. Map showing localities and inferred distributions of the Huckleberry Ridge, Mesa Falls, and Lava Creek ash beds (Pearlette family ash beds) of Pliocene and Pleistocene age in the western United States and southern Canada. *U.S. Geol. Surv. Misc. Investig. Ser. Map* I-1325 https://doi.org/10.3133/i1325 (1982).
38. Rose, W. I. & Chesner, C. A. Dispersal of ash in the great Toba eruption, 75 ka. *Geology* **15**, 913–917 (1987).
39. Cisneros de León, A. et al. A history of violence: magma incubation, timing and tephra distribution of the Los Chocoyos supereruption (Atitlán Caldera, Guatemala). *J. Quat. Sci.* **36**, 169–179 (2021).
40. Nash, B. P., Perkins, M. E., Christensen, J. N., Lee, D. C. & Halliday, A. N. The Yellowstone hotspot in space and time: Nd and Hf isotopes in silicic magmas. *Earth Planet. Sci. Lett.* **247**, 143–156 (2006).
41. Nash, B. P. & Perkins, M. E. Neogene fallout tuffs from the Yellowstone hotspot in the Columbia Plateau region, Oregon, Washington and Idaho, USA. *PLoS One* **7**, e44205 (2012).
42. Matthews, N. E. et al. Ultra-distal tephra deposits from super-eruptions: examples from Toba, Indonesia and Taupo Volcanic Zone, New Zealand. *Quat. Int.* **258**, 54–79 (2012).
43. Pearce, N. J. G., Westgate, J. A., Gualda, G. A. R., Gatti, E. & Muhammad, R. F. Tephra glass chemistry provides storage and discharge details of five magma reservoirs which fed the 75 ka Youngest Toba Tuff eruption, northern Sumatra. *J. Quat. Sci.* **35**, 256–271 (2020).
44. Cooper, G. F., Wilson, C. J. N., Millet, M.-A., Baker, J. & Smith, E. G. C. Systematic tapping of independent magma chambers during the 1 Ma Kidnappers supereruption. *Earth Planet. Sci. Lett.* **213–214**, 23–33 (2012).
45. Carey, S. & Sigurdsson, H. The intensity of plinian eruptions. *Bull. Volcanol.* **51**, 28–40 (1989).
46. Ninkovich, D., Sparks, R. S. J. & Ledbetter, M. T. The exceptional magnitude and intensity of the Toba eruption, Sumatra: an example of the use of deep-sea tephra layers as a geological tool. *Bull. Volcanol.* **41**, 286–298 (1978).
47. Ledbetter, M. T. & Sparks, R. S. J. Duration of large-magnitude explosive eruptions deduced from graded bedding in deep-sea ash layers. *Geology* **7**, 240–244 (1979).
48. Sparks, R. S. J. et al. *Volcanic Plumes* (Wiley, 1997).
49. Baines, P. G. & Sparks, R. S. J. Dynamics of giant volcanic ash clouds from supervolcanic eruptions. *Geophys. Res. Lett.* **32**, L24808 (2005).
50. Costa, A., Suzuki, Y. J. & Koyaguchi, T. Understanding the plume dynamics of explosive super-eruptions. *Nat. Comm.* **9**, 654 (2018).
51. Wilson, C. J. N. & Hildreth, W. The Bishop Tuff: new insights from eruptive stratigraphy. *J. Geol.* **105**, 407–439 (1997).
52. Sheridan, M. F. & Wang, Y. Cooling and welding history of the Bishop Tuff in Adobe Valley and Chidago Canyon, California. *J. Volcanol. Geotherm. Res.* **142**, 119–144 (2005).
53. Wilson, C. J. N. & Hildreth, W. Assembling an ignimbrite: mechanical and thermal building blocks in the Bishop Tuff, California. *J. Geol.* **111**, 653–670 (2003).
54. Brown, S. J. A., Wilson, C. J. N., Cole, J. W. & Wooden, J. The Whakamaru group ignimbrites, Taupo Volcanic Zone, New Zealand: evidence for reverse tapping of a zoned silicic magmatic system. *J. Volcanol. Geotherm. Res.* **84**, 1–37 (1998).

55. Cooper, G. F. & Wilson, C. J. N. Development, mobilisation and eruption of a large crystal-rich rhyolite: the Ongatiti ignimbrite, New Zealand. *Lithos* **198–199**, 38–57 (2014).
56. Cas, R. A. F. et al. The flow dynamics of an extremely large volume pyroclastic flow, the 2.08-Ma Cerro Galán Ignimbrite, NW Argentina, and comparison with other flow types. *Bull. Volcanol.* **73**, 1583–1609 (2011).
57. Wilson, C. J. N. The 26.5 ka Oruanui eruption, New Zealand: an introduction and overview. *J. Volcanol. Geotherm. Res.* **112**, 133–174 (2001).
58. Self, S., Goff, F., Gardner, J. N., Wright, J. V. & Kite, W. M. Explosive rhyolitic volcanism in the Jemez Mountains: vent locations, caldera development and relation to regional structure. *J. Geophys. Res.* **91**, 1779–1798 (1986).
59. Swallow, E. J. et al. Evacuation of multiple magma bodies and the onset of caldera collapse in a supereruption, captured in glass and mineral compositions. *Contrib. Mineral. Petrol.* **173**, 33 (2018).
60. Myers, M. L., Wallace, P. J., Wilson, C. J. N., Morter, B. K. & Swallow, E. J. Prolonged ascent and episodic venting of discrete magma batches at the onset of the Huckleberry Ridge supereruption, Yellowstone. *Earth Planet. Sci. Lett.* **451**, 285–297 (2016).
61. Wilson, C. J. N. & Charlier, B. L. A. Rapid rates of magma generation at contemporaneous magma systems, Taupo volcano, New Zealand: insights from U–Th model-age spectra in zircons. *J. Petrol.* **50**, 875–907 (2009).
62. Wilson, C. J. N., Stelten, M. E. & Lowenstern, J. B. Contrasting perspectives on the Lava Creek Tuff eruption, Yellowstone, from new U–Pb and $^{40}Ar/^{39}Ar$ age determinations. *Bull. Volcanol.* **80**, 53 (2018).
63. Mucek, A. E. et al. Post-supereruption recovery at Toba caldera. *Nat. Comm.* **8**, 15248 (2017).
64. Cooper, G. F., Morgan, D. J. & Wilson, C. J. N. Rapid assembly and rejuvenation of a large silicic magmatic system: insights from mineral diffusive profiles in the Kidnappers and Rocky Hill deposits, New Zealand. *Earth Planet. Sci. Lett.* **473**, 1–13 (2017).
65. Girard, G. & Stix, J. Magma recharge and crystal mush rejuvenation associated with early post-collapse Upper Basin Member rhyolites, Yellowstone caldera, Wyoming. *J. Petrol.* **50**, 2095–2125 (2009).
66. Till, C. B., Vazquez, J. A., Stelten, M. E., Shamloo, H. I. & Shaffer, J. S. Coexisting discrete bodies of rhyolite and punctuated volcanism characterize Yellowstone's post-Lava Creek Tuff caldera evolution. *Geochem. Geophys. Geosyst.* **20**, 3861–3881 (2019).
67. Troch, J., Ellis, B. S., Harris, C., Ulmer, P. & Bachmann, O. The effect of prior hydrothermal alteration on the melting behaviour during rhyolite formation in Yellowstone, and its importance in the generation of low-$\delta^{18}O$ magmas. *Earth Planet. Sci. Lett.* **481**, 338–349 (2018).
68. Cook, G. W., Wolff, J. A. & Self, S. Estimating the eruptive volume of a large pyroclastic body: the Otowi Member of the Bandelier Tuff, Valles caldera, New Mexico. *Bull. Volcanol.* **78**, 10 (2016).
69. Wilson, C. J. N., Gravley, D. M., Leonard, G. S. & Rowland, J. V. Volcanism in the central Taupo Volcanic Zone, New Zealand: tempo, styles and controls. *Spec. Publ. IAVCEI* **2**, 225–247 (2009).
70. Downs, D. T. et al. Age and eruptive center of the Paeroa subgroup ignimbrites (Whakamaru Group) within the Taupo Volcanic Zone of New Zealand. *Geol. Soc. Am. Bull.* **126**, 1131–1144 (2014).
71. Forni, F., Degruyter, W., Bachmann, O., De Astis, G. & Mollo, S. Long-term magmatic evolution reveals the beginning of a new caldera cycle at Campi Flegrei. *Sci. Adv.* **4**, eaat9401 (2018).
72. Townsend, M., Degruyter, W., Huber, C. & Bachmann, O. Magma chamber growth during intercaldera periods: insights from thermo-mechanical modeling with applications to Laguna del Maule, Campi Flegrei, Santorini, and Aso. *Geochem. Geophys. Geosyst.* **20**, 1574–1591 (2019).
73. Riley, P., Tikoff, B. & Hildreth, W. Transtensional deformation and structural control of contiguous but independent magmatic systems: Mono-Inyo Craters, Mammoth Mountain, and Long Valley caldera, California. *Geosphere* **8**, 740–751 (2012).
74. Allan, A. S. R., Wilson, C. J. N., Millet, M.-A. & Wysoczanski, R. J. The invisible hand: tectonic triggering and modulation of a rhyolitic supereruption. *Geology* **40**, 563–566 (2012).
75. Hildreth, W. & Michael, P. J. Comment and reply on 'Chemical differentiation of the Bishop Tuff and other high-silica magmas through crystallization processes'. *Geology* **11**, 622–624 (1983).
76. Bachmann, O. & Bergantz, G. W. Gas percolation in upper-crustal silicic mushes as a mechanism for upward heat advection and rejuvenation of near-solidus magma bodies. *J. Volcanol. Geotherm. Res.* **149**, 85–102 (2006).
77. Huber, C., Bachmann, O. & Dufek, J. Thermo-mechanical reactivation of locked crystal mushes: melting-induced internal fracturing and assimilation processes in magmas. *Earth Planet. Sci. Lett.* **304**, 443–454 (2011).
78. Parmigiani, A., Huber, C. & Bachmann, O. Mush microphysics and the reactivation of crystal-rich magma reservoirs. *J. Geophys. Res. Solid Earth* **119**, 6308–6322 (2014).
79. Wolff, J. A. et al. Remelting of cumulates as a process for producing chemical zoning in silicic tuffs: a comparison of cool, wet and hot, dry rhyolitic magma systems. *Lithos* **236–237**, 275–286 (2015).
80. Streck, M. L. Evaluation of crystal mush extraction models to explain crystal-poor rhyolites. *J. Volcanol. Geotherm. Res.* **284**, 79–94 (2014).
81. Wolff, J. A., Forni, F., Ellis, B. S. & Szymanowski, D. Europium and barium enrichments in compositionally zoned felsic tuffs: a smoking gun for the origin of chemical and physical gradients by cumulate melting. *Earth Planet. Sci. Lett.* **540**, 116251 (2020).
82. Cashman, K. V. & Giordano, G. Calderas and magma reservoirs. *J. Volcanol. Geotherm. Res.* **288**, 28–45 (2014).
Summarizes and synthesizes many of the key concepts in our views of magmatic systems below caldera volcanoes.
83. Lipman, P. W. Subsidence of ash-flow calderas: relation to caldera size and magma-chamber geometry. *Bull. Volcanol.* **59**, 198–218 (1997).
84. Lipman, P. W. & McIntosh, W. C. Eruptive and noneruptive calderas, northeastern San Juan Mountains, Colorado: where did the ignimbrites come from? *Geol. Soc. Am. Bull.* **120**, 771–795 (2008).
85. Gravley, D. M., Wilson, C. J. N., Leonard, G. S. & Cole, J. W. Double trouble: paired ignimbrite eruptions and collateral subsidence in the Taupo Volcanic Zone, New Zealand. *Geol. Soc. Am. Bull.* **119**, 18–30 (2007).
86. Putirka, K. D. & Tepley, F. J. III (eds) Minerals, inclusions and volcanic rocks. *Rev. Mineral. Geochem.* **69**, 1–674 (2008).
87. Gualda, G. A. R., Ghiorso, M. S., Lemons, R. V. & Carley, T. L. Rhyolite-MELTS: a modified calibration of MELTS optimized for silica-rich, fluid-bearing magmatic systems. *J. Petrol.* **53**, 875–890 (2012).
88. Wilke, S., Holtz, F., Neave, D. A. & Almeev, R. The effect of anorthite content and water on quartz–feldspar cotectic compositions in the rhyolitic system and implications for geobarometry. *J. Petrol.* **58**, 789–819 (2017).
89. Huang, H.-H. et al. The Yellowstone magmatic system from the mantle plume to the upper crust. *Science* **348**, 773–776 (2015).
Using tomographic techniques, this paper presented the new discovery at Yellowstone (but now recognized at other centres globally) of the lower-crustal basaltic magma reservoir in addition to the previously known upper-crustal magma reservoir.
90. Jaxybulatov, K. et al. A large magmatic sill complex beneath the Toba caldera. *Science* **346**, 617–619 (2014).
91. Quick, J. E. et al. Magmatic plumbing of a large Permian caldera exposed to a depth of 25 km. *Geology* **37**, 603–606 (2009).
92. Otamendi, J. E., Ducea, M. N. & Bergantz, G. W. Geological, petrological and geochemical evidence for progressive construction of an arc crustal section, Sierra de Valle Fertil, Famatinian Arc, Argentina. *J. Petrol.* **53**, 761–800 (2012).
93. Klein, B. Z. & Jagoutz, O. Construction of a trans-crustal magma system: building the Bear Valley Intrusive Suite, southern Sierra Nevada, California. *Earth Planet. Sci. Lett.* **553**, 116624 (2021).
94. Hildreth, W. & Moorbath, S. Crustal contributions to arc magmatism in the Andes of central Chile. *Contrib. Mineral. Petrol.* **98**, 455–489 (1988).
95. Rowe, M. C. et al. Development of a continental volcanic field: petrogenesis of pre-caldera intermediate and silicic rocks and origin of the Bandelier magmas, Jemez Mountains (New Mexico, USA). *J. Petrol.* **48**, 2063–2091 (2007).
96. Wright, H. M. N., Folkes, C. B., Cas, R. A. F. & Cashman, K. V. Heterogeneous pumice populations in the 2.08-Ma Cerro Galán ignimbrite: implications for magma recharge and ascent preceding a large-volume silicic eruption. *Bull. Volcanol.* **73**, 1513–1533 (2011).
97. Cooper, G. F., Wilson, C. J. N., Millet, M.-A. & Baker, J. A. Generation and rejuvenation of a supervolcanic magmatic system: a case study from Mangakino volcanic centre, New Zealand. *J. Petrol.* **57**, 1135–1170 (2016).
98. Barker, S. J., Wilson, C. J. N., Morgan, D. J. & Rowland, J. V. Rapid priming, accumulation and recharge of magma driving recent eruptions at a hyperactive caldera volcano. *Geology* **44**, 323–326 (2016).
99. Goff, F., Warren, R. G., Goff, C. J. & Dunbar, N. Eruption of reverse-zoned upper Tshirege Member, Bandelier Tuff from centralized vents within Valles caldera, New Mexico. *J. Volcanol. Geotherm. Res.* **276**, 82–104 (2014).
100. Matthews, N. E., Huber, C., Pyle, D. M. & Smith, V. C. Timescales of magma recharge and reactivation of large silicic systems from Ti diffusion in quartz. *J. Petrol.* **53**, 1385–1416 (2012).
101. Shamloo, H. I. & Till, C. B. Decadal transition from quiescence to supereruption: petrologic investigation of the Lava Creek Tuff, Yellowstone Caldera, WY. *Contrib. Mineral. Petrol.* **174**, 32 (2019).
102. Wotzlaw, J.-F., Bindeman, I. N., Stern, R. A., D'Abzac, F.-X. & Schaltegger, U. Rapid heterogeneous assembly of multiple magma reservoirs prior to Yellowstone supereruptions. *Sci. Rep.* **5**, 14026 (2015).
103. Charlier, B. L. A., Wilson, C. J. N. & Davidson, J. P. Rapid open-system assembly of a large silicic magma body: time-resolved evidence from cored plagioclase crystals in the Oruanui eruption deposits, New Zealand. *Contrib. Mineral. Petrol.* **156**, 799–813 (2008).
104. Wolff, J. A. & Ramos, F. C. Processes in caldera-forming high-silica rhyolite magma: Rb–Sr and Pb isotope systematics of the Otowi Member of the Bandelier Tuff, Valles Caldera, New Mexico, USA. *J. Petrol.* **55**, 345–375 (2014).
105. Chamberlain, K. J., Wilson, C. J. N., Wallace, P. J. & Millet, M.-A. Micro-analytical perspectives on the Bishop Tuff and its magma chamber. *J. Petrol.* **56**, 605–640 (2015).
106. Chamberlain, K. J., Wilson, C. J. N., Wooden, J. L., Charlier, B. L. A. & Ireland, T. R. New perspectives on the Bishop Tuff from zircon textures, ages and trace elements. *J. Petrol.* **55**, 395–426 (2014).
107. Cooper, K. M. Time scales and temperatures of crystal storage in magma reservoirs: implications for magma reservoir dynamics. *Philos. Trans. R. Soc. Lond. A* **377**, 20180009 (2019).
108. Cooper, K. M. & Kent, A. J. R. Rapid remobilization of magmatic crystals kept in cold storage. *Nature* **506**, 480–483 (2014).
109. Barboni, M. et al. Warm storage for arc magmas. *Proc. Natl Acad. Sci. USA* **113**, 13959–13964 (2016).
110. Marsh, B. D. On the crystallinity, probability of occurrence, and rheology of lava and magma. *Contrib. Mineral. Petrol.* **78**, 85–98 (1981).
111. Bai, T. et al. Teleseismic tomography of the Laguna del Maule volcanic field in Chile. *J. Geophys. Res. Solid Earth* **125**, e2020JB019449 (2020).
112. Tierney, C. R., Reid, M. R., Vazquez, J. A. & Chesner, C. A. Diverse late-stage crystallization and storage conditions in melt domains from the Youngest Toba Tuff revealed by age and compositional heterogeneity in the last increment of accessory phase growth. *Contrib. Mineral. Petrol.* **174**, 31 (2019).
113. Wallace, P. J., Anderson, A. T. & Davis, A. M. Gradients in H_2O, CO_2, and exsolved gas in a large-volume silicic magma system: interpreting the record preserved in melt inclusions from the Bishop Tuff. *J. Geophys. Res.* **104**, 20097–20122 (1999).
114. Myers, M. L., Wallace, P. J. & Wilson, C. J. N. Inferring magma ascent times and reconstructing conduit processes in rhyolitic explosive eruptions using diffusive losses of hydrogen from melt inclusions. *J. Volcanol. Geotherm. Res.* **369**, 95–112 (2019).
115. Gualda, G. A. R. et al. Timescales of quartz crystallization and the longevity of the Bishop giant magma body. *PLoS One* **7**, e37492 (2012).
116. Roberge, J., Wallace, P. J. & Kent, A. J. R. Magmatic processes in the Bishop Tuff rhyolitic magma based on trace elements in melt inclusions and pumice matrix glass. *Contrib. Mineral. Petrol.* **165**, 237–257 (2013).
117. Flaherty, T. et al. Multiple timescale constraints for high-flux magma chamber assembly prior to the Late Bronze Age eruption of Santorini (Greece). *Contrib. Mineral. Petrol.* **173**, 75 (2018).

118. Tramontano, S., Gualda, G. A. R. & Ghiorso, M. S. Internal triggering of volcanic eruptions: tracking overpressure regimes for giant magma bodies. *Earth Planet. Sci. Lett.* **472**, 142–151 (2017).
119. Kennedy, B. M. et al. Magma plumbing beneath collapse caldera volcanic systems. *Earth-Sci. Rev.* **177**, 404–424 (2018).
120. Black, B. A. & Andrews, B. J. Petrologic imaging of the architecture of magma reservoirs feeding caldera-forming eruptions. *Earth Planet. Sci. Lett.* **552**, 116572 (2020).
121. Vazquez, J. A. & Reid, M. R. Probing the accumulation history of the voluminous Toba magma. *Science* **305**, 991–994 (2004).
122. Matthews, N. E. et al. Quartz zoning and the pre-eruptive evolution of the ~340-ka Whakamaru magma systems, New Zealand. *Contrib. Mineral. Petrol.* **163**, 87–107 (2012).
123. Engi, M. Petrochronology based on REE-minerals: monazite, allanite, xenotime, apatite. *Rev. Mineral. Geochem.* **83**, 365–418 (2017).
124. Kohn, M. J. Titanite petrochronology. *Rev. Mineral. Geochem.* **83**, 419–441 (2017).
125. Schaltegger, U., Schmitt, A. K. & Horstwood, M. S. A. U–Th–Pb zircon geochronology by ID-TIMS, SIMS, and laser ablation ICP-MS: recipes, interpretations, and opportunities. *Chem. Geol.* **402**, 89–110 (2015).
126. Miller, J. S., Matzel, J. E. P., Miller, C. F., Burgess, S. D. & Miller, R. B. Zircon growth and recycling during the assembly of large, composite arc plutons. *J. Volcanol. Geotherm. Res.* **167**, 282–299 (2007).
127. Frazer, R. E., Coleman, D. S. & Mills, R. D. Zircon U-Pb geochronology of the Mount Givens Granodiorite: Implications for the genesis of large volumes of eruptible magma. *J. Geophys. Res. Solid Earth* **119**, 2907–2924 (2014).
128. Cooper, G. F., Wilson, C. J. N., Charlier, B. L. A., Wooden, J. L. & Ireland, T. R. Temporal evolution and compositional signatures of two supervolcanic systems recorded in zircons from Mangakino volcanic centre, New Zealand. *Contrib. Mineral. Petrol.* **167**, 1018 (2014).
129. Rivera, T. A., Schmitz, M. D., Crowley, J. L. & Storey, M. Rapid magma evolution constrained by zircon petrochronology and $^{40}Ar/^{39}Ar$ sanidine ages for the Huckleberry Ridge Tuff, Yellowstone, USA. *Geology* **42**, 643–646 (2014).
130. Charlier, B. L. A. et al. Magma generation at a large, hyperactive silicic volcano (Taupo, New Zealand) revealed by U–Th and U–Pb systematics in zircons. *J. Petrol.* **46**, 3–32 (2005).
131. Folkes, C. B., de Silva, S. L., Schmitt, A. K. & Cas, R. A. F. A reconnaissance of U-Pb zircon ages in the Cerro Galán system, NW Argentina: prolonged magma residence, crystal recycling, and crustal assimilation. *J. Volcanol. Geotherm. Res.* **206**, 136–147 (2011).
132. Reid, M. R. & Vazquez, J. A. Fitful and protracted magma assembly leading to a giant eruption, Youngest Toba Tuff, Indonesia. *Geochem. Geophys. Geosyst.* **18**, 156–177 (2017).
133. Reid, M. R. How long does it take to supersize an eruption? *Elements* **4**, 23–28 (2008).
134. Chamberlain, K. J., Morgan, D. J. & Wilson, C. J. N. Timescales of mixing and mobilisation in the Bishop Tuff magma body: perspectives from diffusion chronometry. *Contrib. Mineral. Petrol.* **168**, 1034 (2014).
135. Costa, F., Shea, T. & Ubide, T. Diffusion chronometry and the timescales of magmatic processes. *Nat. Rev. Earth Environ.* **1**, 201–214 (2020).
136. Druitt, T. H., Costa, F., Deloule, E., Dungan, M. A. & Scaillet, B. Decadal to monthly timescales of magma transfer and reservoir growth at a caldera volcano. *Nature* **482**, 77–80 (2012).
137. Hughes, G. R. & Mahood, G. A. Silicic calderas in arc settings: characteristics, distribution, and tectonic controls. *Geol. Soc. Am. Bull.* **123**, 1577–1595 (2011).
138. Caricchi, L., Annen, C., Blundy, J., Simpson, G. & Pinel, V. Frequency and magnitude of volcanic eruptions controlled by magma injection and buoyancy. *Nat. Geosci.* **7**, 126–130 (2014).
139. Koulakov, I. et al. The feeder system of the Toba supervolcano from the slab to the shallow reservoir. *Nat. Comm.* **7**, 12228 (2016).
140. Rowland, J. V., Wilson, C. J. N. & Gravley, D. M. Spatial and temporal variations in magma-assisted rifting, Taupo Volcanic Zone, New Zealand. *J. Volcanol. Geotherm. Res.* **190**, 89–108 (2010).
141. Heath, B. A. et al. Tectonism and its relation to magmatism around Santorini volcano from upper crustal *P* wave velocity. *J. Geophys. Res. Solid Earth* **124**, 10610–10629 (2019).
142. Peterson, D. E. et al. Active normal faulting, diking, and doming above the rapidly inflating Laguna del Maule volcanic field, Chile, imaged with CHIRP, magnetic, and focal mechanism data. *J. Geophys. Res. Solid Earth* **125**, e2019JB019329 (2020).
143. Cole, J. W., Milner, D. M. & Spinks, K. D. Calderas and caldera structures: a review. *Earth-Sci. Rev.* **69**, 1–26 (2005).
144. Rowland, J. V. & Sibson, R. H. Extensional fault kinematics within the Taupo Volcanic Zone, New Zealand: soft-linked segmentation of a continental rift system. *New Zealand J. Geol. Geophys.* **44**, 271–283 (2001).
145. Heise, W., Caldwell, T. G., Bibby, H. M. & Bennie, S. L. Three-dimensional electrical resistivity image of magma beneath an active continental rift, Taupo Volcanic Zone, New Zealand. *Geophys. Res. Lett.* **37**, L10301 (2010).
146. Flinders, A. F. et al. Seismic evidence for significant melt beneath the Long Valley Caldera, California, USA. *Geology* **46**, 799–802 (2018).
147. Hammond, J. O. S. & Kendall, J.-M. Constraints on melt distribution from seismology: a case study in Ethiopia. *Geol. Soc. Lond. Spec. Publ.* **420**, 127–147 (2016).
148. Rasht-Behesht, M., Huber, C. & Mancinelli, N. J. Detectability of melt-rich lenses in magmatic reservoirs from teleseismic waveform modeling. *J. Geophys. Res. Solid Earth* **125**, e2020JB020264 (2020).
149. Lowenstern, J., Sisson, T. & Hurwitz, S. Probing magma reservoirs to improve volcano forecasts. *Eos* https://doi.org/10.1029/2017EO085189 (2017).
150. Lowenstern, J. B., Smith, R. B. & Hill, D. P. Monitoring super-volcanoes: geophysical and geochemical signals at Yellowstone and other large caldera systems. *Philos. Trans. R. Soc. Lond. A* **364**, 2055–2072 (2006).
151. Lehman, J. A., Smith, R. B. & Schilly, M. M. Upper crustal structure of the Yellowstone caldera from seismic delay time analyses and gravity correlations. *J. Geophys. Res.* **87**, 2713–2730 (1982).
152. Miller, D. S. & Smith, R. B. *P* and *S* velocity structure of the Yellowstone volcanic field from local earthquake and controlled source tomography. *J. Geophys. Res.* **104**, 15105–15121 (1999).
153. Husen, S., Smith, R. B. & Waite, G. P. Evidence for gas and magmatic sources beneath the Yellowstone volcanic field from seismic tomographic imaging. *J. Volcanol. Geotherm. Res.* **131**, 397–410 (2004).
154. Farrell, J., Smith, R. B., Husen, S. & Diehl, T. Tomography from 26 years of seismicity revealing that the spatial extent of the Yellowstone crustal magma reservoir extends well beyond the Yellowstone caldera. *Geophys. Res. Lett.* **41**, 3068–3073 (2014).
155. Seats, K. J. & Lawrence, J. F. The seismic structure beneath the Yellowstone Volcano Field from ambient seismic noise. *Geophys. Res. Lett.* **41**, 8277–8282 (2014).
156. Jiang, C., Schmandt, B., Farrell, J., Lin, F.-C. & Ward, K. M. Seismically anisotropic magma reservoirs underlying silicic calderas. *Geology* **46**, 727–730 (2018).
157. Singer, B. S. et al. Geomorphic expression of rapid Holocene silicic magma reservoir growth beneath Laguna del Maule, Chile. *Sci. Adv.* **4**, eaat1513 (2018).
158. Hata, M. et al. Three-dimensional electrical resistivity modeling to elucidate the crustal magma supply system beneath Aso caldera, Japan. *J. Geophys. Res. Solid Earth* **123**, 6334–6346 (2018).
159. Hill, D. P., Montgomery-Brown, E. K., Shelly, D. R., Flinders, A. F. & Prejean, S. Post-1978 tumescence at Long Valley caldera, California: a geophysical perspective. *J. Volcanol. Geotherm. Res.* **400**, 106900 (2020).
160. Hildreth, W. Fluid-driven uplift at Long Valley, California: geologic perspectives. *J. Volcanol. Geotherm. Res.* **341**, 269–286 (2017).
161. Prudencio, J. & Manga, M. 3-D seismic attenuation structure of Long Valley caldera: looking for melt bodies in the shallow crust. *Geophys. J. Int.* **220**, 1677–1686 (2020).
162. Wilson, C. J. N. Stratigraphy, chronology, styles and dynamics of late Quaternary eruptions from Taupo volcano, New Zealand. *Philos. Trans. R. Soc. Lond. A* **343**, 205–306 (1993).
163. Acocella, V., Di Lorenzo, R., Newhall, C. & Scandone, R. An overview of recent (1988 to 2014) caldera unrest: Knowledge and perspectives. *Rev. Geophys.* **53**, 896–955 (2015).
This paper provides an extensive review of global caldera unrest, both eruptive and non-eruptive, highlighting the diversity and complexity in the causes and signals of unrest.
164. Yellowstone Volcano Observatory. Volcano and earthquake monitoring plan for the Yellowstone Volcano Observatory, 2006–2015. *U.S. Geol. Surv. Sci. Investig. Rep.* **2006–5276**, 1–13 (2006).
165. Waite, G. P. & Smith, R. B. Seismic evidence for fluid migration accompanying subsidence of the Yellowstone caldera. *J. Geophys. Res.* **107**, 2177 (2002).
166. Farrell, J., Smith, R. B., Taira, T., Chang, W. L. & Puskas, C. M. Dynamics and rapid migration of the energetic 2008–2009 Yellowstone Lake earthquake swarm. *Geophys. Res. Lett.* **37**, L19305 (2010).
167. Massin, F., Farrell, J. & Smith, R. B. Repeating earthquakes in the Yellowstone volcanic field: Implications for rupture dynamics, ground deformation, and migration in earthquake swarms. *J. Volcanol. Geotherm. Res.* **257**, 159–173 (2013).
168. Pang, G. et al. The 2017–2018 Maple Creek earthquake sequence in Yellowstone National Park, USA. *Geophys. Res. Lett.* **46**, 4653–4663 (2019).
169. Wicks, C., Thatcher, W., Dzurisin, D. & Svarc, J. Uplift, thermal unrest and magma intrusion at Yellowstone caldera. *Nature* **440**, 72–75 (2006).
170. Wicks, C., Dzurisin, D., Lowenstern, J. B. & Svarc, J. Magma intrusion and volatile ascent beneath Norris Geyser Basin, Yellowstone National Park. *J. Geophys. Res. Solid Earth* **125**, e2019JB018208 (2020).
171. Chang, W.-L., Smith, R. B., Farrell, J. & Puskas, C. M. An extraordinary episode of Yellowstone caldera uplift, 2004–2010, from GPS and InSAR observations. *Geophys. Res. Lett.* **37**, L23302 (2010).
172. Langbein, J. O. Deformation of the Long Valley caldera, California: inferences from measurements from 1988 to 2001. *J. Volcanol. Geotherm. Res.* **127**, 247–267 (2003).
173. Feng, L. & Newman, A. V. Constraints on continued episodic inflation at Long Valley caldera, based on seismic and geodetic observations. *J. Geophys. Res.* **114**, B06403 (2009).
174. Tizzani, P. et al. Uplift and magma intrusion at Long Valley caldera from InSAR and gravity measurements. *Geology* **37**, 63–66 (2009).
175. Johnston, D. et al. Social and economic consequences of historic caldera unrest at the Taupo volcano, New Zealand and the management of future episodes of unrest. *Bull. New Zealand Soc. Earthq. Eng.* **35**, 215–230 (2002).
176. Otway, P. M., Blick, G. H. & Scott, B. J. Vertical deformation at Lake Taupo, New Zealand, from lake levelling surveys, 1979–99. *New Zealand J. Geol. Geophys.* **45**, 121–132 (2002).
177. Illsley-Kemp, F. et al. Volcanic unrest at Taupō volcano in 2019: causes, mechanisms and implications. *Geochem. Geophys. Geosyst.* **22**, e2021GC009803 (2021).
178. Bellucci, F., Woo, J., Kilburn, C. R. J. & Rolandi, G. Ground deformation at Campi Flegrei, Italy: implications for hazard assessment. *Geol. Soc. Lond. Spec. Publ.* **269**, 141–157 (2006).
179. De Natale, G. et al. The Campi Flegrei caldera: unrest mechanisms and hazards. *Geol. Soc. Lond. Spec. Publ.* **269**, 25–45 (2006).
180. Wilson, C. J. N. Volcanoes: characteristics, tipping points and those pesky unknown unknowns. *Elements* **13**, 41–46 (2017).
181. Atwood, E. *Cultural Super Volcano: a Cultural History of Yellowstone's Hot Spot via Eco-Paranoia*. Thesis, Montana State Univ., (2020).
182. Kong, Q. et al. Machine learning in seismology: turning data into insights. *Seismol. Res. Lett.* **90**, 3–14 (2019).
183. Myers, M. L., Wallace, P. J., Wilson, C. J. N., Watkins, J. L. & Liu, Y. Ascent rates of rhyolitic magma at the onset of three caldera-forming eruptions. *Am. Mineral.* **103**, 952–965 (2018).
184. Freitas, D., Manthilake, G. & Chantel, J. Simultaneous measurements of electrical conductivity and seismic wave velocity of partially molten geological materials: effect of evolving melt texture. *Phys. Chem. Mineral.* **46**, 535–551 (2019).
185. Carcione, J. M., Farina, B., Poletto, F., Qadrouh, A. N. & Cheng, W. Seismic attenuation in partially molten rocks. *Phys. Earth Planet. Int.* **309**, 106568 (2020).
186. Barberi, F., Corrado, G., Innocenti, F. & Luongo, G. Phlegraean Fields 1982–1984: brief chronicle of a volcano emergency in a densely populated area. *Bull. Volcanol.* **47**, 175–185 (1984).

187. Maj, M. et al. Prevalence of psychiatric disorders among subjects exposed to a natural disaster. *Acta Psychol. Scand.* **79**, 544–549 (1989).
188. Longo, M. L. How memory can reduce the vulnerability to disasters: the bradyseism of Pozzuoli in southern Italy. *AIMS Geosci.* **5**, 631–644 (2019).
189. Chesner, C. A. Petrogenesis of the Toba Tuffs, Sumatra, Indonesia. *J. Petrol.* **39**, 397–438 (1998).
190. Rose, W. I., Grant, N. K. & Easter, J. Geochemistry of the Los Chocoyos ash, Quezaltenango Valley, Guatemala. *Geol. Soc. Am. Spec. Pap.* **180**, 87–99 (1979).
191. Takarada, S. & Hoshizumi, H. Distribution and eruptive volume of Aso-4 pyroclastic density current and tephra fall deposits, Japan: A M8 super-eruption. *Front. Earth Sci.* **8**, 170 (2020).
192. Keller, F., Bachmann, O., Geshi, N. & Miyakawa, A. The role of crystal accumulation and cumulate remobilization in the formation of large zoned ignimbrites: insights from the Aso-4 caldera-forming eruption, Kyushu, Japan. *Front. Earth Sci.* **8**, 614267 (2021).
193. Matthews, N. E., Vazquez, J. A. & Calvert, A. T. Age of the Lava Creek supereruption and magma chamber assembly at Yellowstone based on $^{40}Ar/^{39}Ar$ and U-Pb dating of sanidine and zircon crystals. *Geochem. Geophys. Geosyst.* **16**, 2508–2528 (2015).
194. Crowley, J. L., Schoene, B. & Bowring, S. A. U-Pb dating of zircon in the Bishop Tuff at the millennial scale. *Geology* **35**, 1123–1126 (2007).
195. Jolles, J. S. R. & Lange, R. A. High-resolution Fe–Ti oxide thermometry applied to single-clast pumices from the Bishop Tuff: a re-examination of compositional variations in phenocryst phases with temperature. *Contrib. Mineral. Petrol.* **174**, 70 (2019).
196. Wu, J. et al. Crustal evolution leading to successive rhyolitic supereruptions in the Jemez Mountains volcanic field, New Mexico, USA. *Lithos* **396–397**, 106201 (2021).
197. Cherniak, D. J. & Watson, E. B. Pb diffusion in zircon. *Chem. Geol.* **172**, 5–24 (2000).
198. Ireland, T. R. & Williams, I. S. Considerations in zircon geochronology by SIMS. *Rev. Mineral. Geochem.* **53**, 215–241 (2003).
199. Schmitt, A. K. & Vazquez, J. A. Secondary ionization mass spectrometry analysis in petrochronology. *Rev. Mineral. Geochem.* **83**, 199–230 (2017).
200. Liu, Y. et al. Reappraisement and refinement of zircon U-Pb isotope and trace element analyses by LA-ICP-MS. *Chin. Sci. Bull.* **55**, 1535–1546 (2010).
201. Chang, Z., Vervoort, J. D., McClelland, W. C. & Knaack, C. U-Pb dating of zircon by LA-ICP-MS. *Geochem. Geophys. Geosyst.* **7**, Q05009 (2006).

Acknowledgements
C.J.N.W. has been supported by the Marsden Fund grant VUW0813 (Royal Society of New Zealand), a James Cook Fellowship (Royal Society of New Zealand) and the ECLIPSE Programme, funded by the New Zealand Ministry of Business, Innovation and Employment. G.F.C. is supported by a NERC Standard Grant (NE/T000317/1), M.L.M. is supported by an NSF CAREER grant (EAR 2042662) and S.J.B. acknowledges Marsden Fund grant VUW1627.

Author contributions
G.F.C. and K.J.C. conceived the idea of the manuscript. All authors drafted the manuscript, led by C.J.N.W. All authors commented on and discussed the manuscript at all stages.

Competing interests
The authors declare no competing interests.

Peer review information
Nature Reviews Earth & Environment thanks J. Lindsay and O. Bachmann (who co-reviewed with F. Keller) for their contribution to the peer review of this work.

Publisher's note
Springer Nature remains neutral with regard to jurisdictional claims in published maps and institutional affiliations.